Perturbation of a Schwarzschild Black Hole Due to a Rotating Thin Disk

P. Čížek and O. Semerák

Institute of Theoretical Physics, Faculty of Mathematics and Physics, Charles University, Prague, Czech Republic; oldrich.semerak@mff.cuni.cz

Abstract

Will, in 1974, treated the perturbation of a Schwarzschild black hole due to a slowly rotating, light, concentric thin ring by solving the perturbation equations in terms of a multipole expansion of the mass-and-rotation perturbation series. In the Schwarzschild background, his approach can be generalized to perturbation by a thin disk (which is more relevant astrophysically), but, due to rather bad convergence properties, the resulting expansions are not suitable for specific (numerical) computations. However, we show that Green's functions, represented by Will's result, can be expressed in closed form (without multipole expansion), which is more useful. In particular, they can be integrated out over the source (a thin disk in our case) to yield good converging series both for the gravitational potential and for the dragging angular velocity. The procedure is demonstrated, in the first perturbation order, on the simplest case of a constant-density disk, including the physical interpretation of the results in terms of a one-component perfect fluid or a two-component dust in a circular orbit about the central black hole. Free parameters are chosen in such a way that the resulting black hole has zero angular momentum but non-zero angular velocity, as it is just carried along by the dragging effect of the disk.

Key words: accretion, accretion disks – black hole physics – gravitation

1. Introduction

Disk-like structures around very compact bodies are likely to play a key role in the most energetic astrophysical sources like active galactic nuclei, X-ray binaries, supernovae, and gamma-ray bursts. Analytical modeling of such structures relies on various simplifying assumptions, the basic ones being their stationarity, axial symmetry, and test (non-gravitating) nature (see, e.g., Kato et al. 2008). The last assumption is justified by two arguments: (i) in the above astrophysical systems, the mass of the disk is typically much smaller than that of the black hole (or neutron star) in their center, so the latter surely dominates the gravitational potential as well as the "radial" field, and (ii) black holes are the strongest possible (extended) gravitational sources (and neutron stars are just slightly less compact), so they would—at least in a certain region—dominate the field even if their mass were less than that of the surrounding matter. However, such arguments need not hold for a latitudinal component of the field (namely, perpendicular to the disk),[1] and most importantly, the additional matter may in fact dominate the second and higher derivatives of the metric (curvature). These higher derivatives are in turn crucial for the stability of the matter's motion, and thus the tricky issue of self-gravity enters the problem. Actually, real, massive matter may thus assume a quite different configuration from test matter (Abramowicz et al. 1984). One should also add that even if the accreting matter really only had a tiny effect on the geometry, it could still significantly change the observational record of the source; in particular, it may change the long-term dynamics of bodies orbiting in the system (e.g., Suková & Semerák 2013 and references therein).

Hence, the properties of accretion systems may be sensitive to the precise shape of the field (Semerák 2003, 2004). Unfortunately, general relativity is nonlinear, and the fields of multiple sources mostly cannot be obtained by simple superposition. Such more complicated fields are being successfully treated numerically (this even applies to strongly time-dependent cases including gravitational collapse, collisions, and waves), but, for the present, the compass of explicit analytical solutions terminates at systems with a very high degree of symmetry, practically at static and axially symmetric cases. It would be most desirable to extend this to *stationary* cases, namely, those admitting rotation. The stationary axisymmetric problem is usually represented in the form of the Ernst equation, but what is actually being tackled is the corresponding linear problem (the Lax pair of equations whose integrability condition is just the Ernst equation). Exact solutions of this problem have been searched for in several ways. Klein & Richter (2005) and Meinel et al. (2008) summarized a "straightforward" but rather involved treatment of the respective boundary-value problems, providing both the black hole and thin-disk solutions, plus prospects of how to also obtain their nonlinear superpositions. Other attempts employed "solution-generating" techniques—mathematical procedures that transform one stationary axisymmetric metric into another and can in principle provide any solution of this type. The practical power of these methods strongly depends on how simple is the "seed" metric, so these methods usually start from a static one. Using the soliton (inverse-scattering) method of Belinsky and Zakharov, Tomimatsu (1984), Krori & Bhattacharjee (1990), Chaudhuri & Das (1997), and Zellerin & Semerák (2000) generated black holes immersed in external fields, but at least the case corresponding to a hole surrounded by a thin disk (Zellerin & Semerák 2000) turned out to be unphysical (Semerák 2002). Bretón et al. (1997), who started from a different representation of the static axisymmetric seed and managed to "install" a rotating black hole in it (see also Bretón et al. 1998 for a charged generalization) seem to have been more successful.

If the external-matter gravity is weak, the problem may be treated as a small perturbation of the central-source metric, which is determined by the linearized Einstein equations. In doing so, one can restrict the problem to special types of perturbations, for

---

[1] For a Schwarzschild black hole, which is spherically symmetric, there is of course no latitudinal field, so any additional source would automatically dominate this component.

example, to stationary and axisymmetric ones. The method can be iterated; in a limit case (many iterations), it goes over to a solution in terms of series. The result then need not represent any longer a tiny variation of any "almost right" metric: it may even be put together on a Minkowski background, with the "strong" part (e.g., a black hole) "dissolved" within the fundamental systems of equations. The main problem with this scheme is the convergence and meaning of the series.

Forty-three years ago, the paper by Will (1974), published in this journal, became a seminal reference on the subject. It provided the gravitational field of a light and slowly rotating thin equatorial ring around a (originally Schwarzschild) black hole by mass-and-rotational perturbation of the Schwarzschild metric. (See also the succeeding paper, Will 1975, where basic properties of the obtained solution were discussed.) Unfortunately, the perturbation-scheme success depends strongly on how simple the background metric is —and the Schwarzschild metric is exceptionally simple: Will's procedure cannot be simply extended to a Kerr background. Consequently, only partial questions have been answered explicitly in this direction, in particular the one regarding the deformation of the Kerr black hole horizon (Chrzanowski 1976; Demianski 1976; interestingly, these two results do not agree on certain points, mainly in the limit of an extreme black hole).[2]

Recently, Will's black hole–ring problem was revisited by Sano & Tagoshi (2014), this time using the perturbation approach of Chrzanowski, Cohen, and Kegeles, in which the metric is found on the basis of the solution of the Teukolsky equation for the Weyl scalars. Will's results have also been followed by Hod, who analyzed the behavior of the innermost stable circular orbit in the black hole–ring field (Hod 2014) and the relation between the angular velocity of the horizon, and the black hole and ring angular momenta (Hod 2015).

In the present paper, we check whether Will's scheme can be adapted to the case of a thin equatorial stationary and axisymmetric disk. (Preliminary results were presented in Čížek & Semerák 2009 and Čížek 2011.) In converging to a positive answer, we first observe that the expansions in spherical harmonics that typically come out in this approach (even in computing just the linear terms) converge rather badly, and their numerical processing is problematic. Much more effective is the use of the Green's functions of the problem, namely, the perturbations generated by an infinitesimal ring. We have been able to express Green's functions in such a way that the linear perturbation due to a thin disk can be obtained in closed form.

This paper is organized as follows. In Section 2, we introduce the equations describing the gravitational field of a thin disk. Section 3 summarizes Will's approach, and Section 4 discusses its (un)suitability for a numerical treatment. In Section 5, we compute the Green's functions of the problem in closed form, and in Section 6 we show, on *linear* perturbation by a thin annular concentric disk, that they can be integrated in order to obtain a perturbation generated by a given (stationary and axisymmetric) distribution of mass. The resulting series converge much better and allow specific configurations to be computed explicitly.

For our notations and conventions: our metric signature is $(-+++)$ and geometrized units are used, in which $c = G = 1$; Greek indices run from 0 to 3, and the partial derivative is denoted by a comma. Complete elliptic integrals are given in terms of the modulus k, so

$$K(k) := \int_0^{\frac{\pi}{2}} \frac{d\alpha}{\sqrt{1 - k^2 \sin^2 \alpha}}, \quad E(k) := \int_0^{\frac{\pi}{2}} \sqrt{1 - k^2 \sin^2 \alpha}\, d\alpha, \quad \Pi(n, k) := \int_0^{\frac{\pi}{2}} \frac{d\alpha}{(1 - n \sin^2 \alpha)\sqrt{1 - k^2 \sin^2 \alpha}}.$$

2. Black Hole and Thin-disk System: Einstein Equations and Boundary Conditions

We will search for the black hole–disk field by perturbation of the Schwarzschild metric, while restricting the search to the simplest spacetimes that can host *rotating* sources, namely, to those which are stationary and axially symmetric. In addition, we will consider asymptotically flat spacetimes, without a cosmological term, and will require their orthogonal transitivity (i.e., the motion of the sources will be limited to stationary circular orbits). In such spacetimes, the time and axial Killing vector fields $\eta^\mu = \frac{\partial x^\mu}{\partial t}$ and $\xi^\mu = \frac{\partial x^\mu}{\partial \phi}$ exist and commute, and the planes tangent to the meridional directions (locally orthogonal to both Killing vectors) are integrable. Needless to say, it is assumed that there exists an axis of space-like symmetry, namely, a connected 2D (time-like) set of fixed points of space-like isometry. In isotropic-type spheroidal coordinates (t, r, θ, ϕ) (of which t and ϕ have been chosen as parameters of the Killing symmetries), the metric with these properties can, for instance, be written in the "Carter–Thorne–Bardeen" form (e.g., Bardeen 1973),

$$ds^2 = -e^{2\nu}dt^2 + B^2 r^2 e^{-2\nu} \sin^2\theta\, (d\phi - \omega dt)^2 + e^{2\zeta - 2\nu}(dr^2 + r^2 d\theta^2), \tag{1}$$

where the unknown functions ν, B, ω, and ζ depend only on r and θ covering the meridional surfaces. Besides the above coordinates, we will also occasionally use the Weyl-type cylindrical coordinates $\rho = r \sin\theta$ and $z = r \cos\theta$.

Apart from the asymptotic flatness, the boundary conditions have to be fixed on the symmetry axis, on the black hole horizon, and on the external-source surface. Regularity of the axis (local flatness of the orthogonal surfaces $z = $ const at $\rho = 0$) requires that $e^\zeta \to B$ at $\rho \to 0^+$. The invariants $g_{tt} = g_{\alpha\beta}\eta^\alpha \eta^\beta$, $g_{t\phi} = g_{\alpha\beta}\eta^\alpha \xi^\beta$, and $g_{\phi\phi} = g_{\alpha\beta}\xi^\alpha \xi^\beta$ have to be even functions of ρ (in order not to induce a conical singularity on the axis). Should the circumferential radius $\sqrt{g_{\phi\phi}}$ grow linearly with proper cylindrical radius ρ $[e^{\zeta - \nu}]_{\rho = 0}$, thus with ρ, there must be $g_{\phi\phi} \approx O(\rho^2)$, and demanding the finiteness of ω, also $-g_{t\phi} = g_{\phi\phi}\omega \approx O(\rho^2)$.

The stationary horizon is characterized by $e^{2\nu} = 0$ and $\omega = $ const $=: \omega_H$ (in our coordinates, it specifically means that $\omega_{,\theta} = 0$ there). In order for the azimuthal and latitudinal circumferences of the horizon to be positive and finite, the functions $Bre^{-2\nu}$ and $e^{2\zeta - 2\nu}$ have

---

[2] Note that another approximation possibility is the post-Newtonian expansion. The composition of a rotating gravitational center with a massive ring in Keplerian rotation was tackled, using the gravito-electromagnetic analogy, by Ruggiero (2016).

to be positive and finite: the latter ensures the regularity of g_{rr} as well. Hence, $Br = 0$ and $e^{2\zeta} = 0$ on the horizon. (Let us add in advance that the field equations also imply that $\omega_{,r}/B$ and $\nu_{,r}\omega_{,r}$ have to be finite on the horizon, so $\omega_{,r}$ has to vanish there as well.)

Now for boundary conditions on the external source. We assume that the latter has the form of an infinitesimally thin disk in the equatorial plane $z = 0$, stretching over some interval of radii lying above the central black hole horizon. We assume that the disk bears neither charge nor current (there are no EM fields) and that the spacetime is reflection-symmetric with respect to its plane. The metric is then continuous everywhere, but has finite jumps in the first normal derivatives $g_{\alpha\beta,z}$ across the disk. The functions ν, B, ω, and ζ must be even in z, their z-derivatives odd in z, and even powers and multiples of derivatives (for example, $B_{,z}\nu_{,z}$) even in z (therefore, they do not jump across $z = 0$).

In order for the spacetime to be stationary, axially symmetric, and orthogonally transitive, the disk elements must only move along surfaces spanned by the Killing fields, namely, they must follow spatially circular orbits with steady angular velocity $\Omega = \frac{d\phi}{dt}$. This corresponds to the four-velocity

$$u^\alpha = \frac{\eta^\alpha + \Omega\xi^\alpha}{|\eta^\alpha + \Omega\xi^\alpha|} = u^t(1, 0, 0, \Omega), \quad u_\alpha = -u^t e^{2\nu}\delta^t_\alpha + u^t B\rho v(-\omega, 0, 0, 1) \tag{2}$$

with

$$(u^t)^2 = \frac{e^{-2\nu}}{1 - B^2\rho^2 e^{-4\nu}(\Omega - \omega)^2} = \frac{e^{-2\nu}}{1 - v^2}, \quad \text{where} \quad v := B\rho e^{-2\nu}(\Omega - \omega) = \sqrt{g_{\phi\phi}}\, e^{-\nu}(\Omega - \omega)$$

represents the linear velocity with respect to the local zero-angular-momentum observer. For the thin disks ($T^z_z = 0$, $T^\rho_z = 0$) without radial pressure ($T^\rho_\rho = 0$), the surface energy-momentum tensor

$$\int_{-\infty}^{\infty} T^\alpha_\beta g_{zz}\, dz = \int_{z=0^-}^{z=0^+} T^\alpha_\beta e^{2\zeta - 2\nu} dz =: S^\alpha_\beta(\rho) \iff T^\alpha_\beta e^{2\zeta - 2\nu} =: S^\alpha_\beta(\rho)\delta(z) \tag{3}$$

has only three non-zero components ($S^t_t, S^t_\phi, S^\phi_\phi$), representing energy density, orbital-momentum density, and azimuthal pressure, respectively. If $(S^\phi_\phi - S^t_t)^2 + 4S^t_\phi S^\phi_t \geqslant 0$, it can be diagonalized to $S^{\alpha\beta} = \sigma u^\alpha u^\beta + P w^\alpha w^\beta$, where σ and P (more precisely, $\sigma e^{\nu-\zeta}$ and $Pe^{\nu-\zeta}$) stand for the surface density and azimuthal pressure in a co-moving frame, and w^α is the "azimuthal" vector perpendicular to u^α, with components $w^\alpha = \frac{1}{\rho B}(u_\phi, 0, 0, -u_t)$, $w_\alpha = \rho B(-u^\phi, 0, 0, u^t)$. Hence, the surface-tensor components read

$$S^t_t = -\sigma - (\sigma + P)u^\phi u_\phi, \quad S^t_\phi = (\sigma + P)u^t u_\phi, \quad S^\phi_\phi = P + (\sigma + P)u^\phi u_\phi. \tag{4}$$

Orthogonally transitive stationary and axisymmetric spacetimes are described by five independent Einstein equations. In our case of a thin disk, the energy-momentum tensor only has the T^t_t, T^t_ϕ, and T^ϕ_ϕ components, and the equations read[3]

$$\nabla \cdot (\rho\nabla B) = 0, \tag{5}$$

$$\nabla \cdot (B\nabla\nu) - \frac{B^3\rho^2}{2e^{4\nu}}(\nabla\omega)^2 = 4\pi B e^{2\zeta-2\nu}(T^\phi_\phi - 2\omega T^t_\phi - T^t_t) = 4\pi B(\sigma + P)\frac{1 + v^2}{1 - v^2}\,\delta(z), \tag{6}$$

$$\nabla \cdot (B^3\rho^2 e^{-4\nu}\nabla\omega) = -16\pi B e^{2\zeta-2\nu}T^t_\phi = -16\pi B^2\rho e^{-2\nu}(\sigma + P)\frac{v}{1 - v^2}\,\delta(z), \tag{7}$$

$$\zeta_{,\rho\rho} + \zeta_{,zz} + (\nu_{,\rho})^2 + (\nu_{,z})^2 - \frac{3B^2\rho^2}{4e^{4\nu}}[(\omega_{,\rho})^2 + (\omega_{,z})^2] = 8\pi e^{2\zeta-2\nu}(T^\phi_\phi - \omega T^t_\phi) = 8\pi\frac{\sigma v^2 + P}{1 - v^2}\,\delta(z), \tag{8}$$

$$\zeta_{,\rho}(B\rho)_{,\rho} - \zeta_{,z}(B\rho)_{,z} = -B\rho[(\nu_{,\rho})^2 - (\nu_{,z})^2] - \frac{1}{2}[(B\rho)_{,\rho\rho} - (B\rho)_{,zz}] + \frac{1}{4}B^3\rho^3 e^{-4\nu}[(\omega_{,\rho})^2 - (\omega_{,z})^2], \tag{9}$$

$$\zeta_{,\rho}(B\rho)_{,z} + \zeta_{,z}(B\rho)_{,\rho} = -2B\rho\nu_{,\rho}\nu_{,z} - (B\rho)_{,\rho z} + \frac{1}{2}B^3\rho^3 e^{-4\nu}\omega_{,\rho}\omega_{,z}, \tag{10}$$

where ∇ and $\nabla\cdot$ denote the gradient and divergence in a (auxiliary) Euclidean three-space. The last two equations (for ζ) are integrable, provided the first three vacuum equations hold. The axis boundary condition $e^\zeta = B$ implies that the ζ function can elsewhere be obtained according to $\zeta(r, \theta) = \int_0^\theta \zeta_{,\theta}d\zeta + \ln B$, where $\zeta_{,\theta}$ follows from the last two field equations.

The treatment of the stationary axisymmetric problem, Equations (5)–(10), usually starts from a suitable solution of the first Equation (5). In the parametrization (coordinates) we use here, it is convenient to choose[4]

$$B = 1 - \frac{k^2}{4r^2}. \tag{11}$$

---

[3]   Equation (8) is *not* independent, but we include it here since it provides the jump of $\zeta_{,z}$ across the equatorial plane given later in Section 2.2.

[4]   When working in Weyl-type coordinates (t, ρ, z, ϕ) and with the corresponding Weyl–Lewis–Papapetrou form of the metric, the B-equation is usually satisfied by $B = 1$. This choice is advantageous in most respects, but it makes the horizon "degenerate" to a central segment of the symmetry axis $\rho = 0$, which is not suitable for a discussion of its properties. Different solutions for B are also possible for the "Carter–Thorne–Bardeen" form of the metric we use here; however, changing B generally does not imply a real physical difference—it effectively corresponds to a certain redefinition of coordinates, cf. Section 6.1 (only the $B = 1/\rho$ choice leads to different, plane-wave solutions).

With such a choice, the horizon lies where $B = 0$, hence on $r = k/2$. This reveals the meaning of the constant k (which is supposed to be positive); in particular, for a Schwarzschild metric, one has $k = M$; for Kerr, it would be $k = M + \sqrt{M^2 - a^2}$, with a the center's specific angular momentum ($k = 0$ would correspond to an extreme black hole, or to a Minkowski spacetime).

The main task is to solve the coupled Equations (6) and (7), and then to integrate Equations (9) and (10) for ζ. With the choice $B = 1 - \frac{k^2}{4r^2}$ (thus with $B_{,\theta} = 0$) and written out explicitly in the (t, ρ, z, ϕ) coordinates, these equations read

$$(r^2 \nu_{,r})_{,r} + r^2 \nu_{,r} (\ln B)_{,r} + \nu_{,\theta\theta} + \nu_{,\theta} \cot \theta = \frac{B^2 r^2}{2 e^{4\nu}} \sin^2 \theta [r^2 (\omega_{,r})^2 + (\omega_{,\theta})^2] + 4\pi r^2 (\sigma + P) \frac{1 + v^2}{1 - v^2} \delta(z), \tag{12}$$

$$r^2 \omega_{,rr} + 4r \omega_{,r}(1 - r\nu_{,r}) + 3r^2 \omega_{,r}(\ln B)_{,r} + \omega_{,\theta\theta} + 3\omega_{,\theta} \cot \theta - 4\omega_{,\theta} \nu_{,\theta} = -\frac{16\pi r e^{2\nu}}{B \sin \theta}(\sigma + P) \frac{v}{1 - v^2} \delta(z), \tag{13}$$

$$(2 - B)r\zeta_{,r} - B\zeta_{,\theta} \cot \theta = B[r^2 (\nu_{,r})^2 - (\nu_{,\theta})^2] + 2B - 2 - \frac{1}{4} B^3 r^2 e^{-4\nu} \sin^2 \theta [r^2 (\omega_{,r})^2 - (\omega_{,\theta})^2], \tag{14}$$

$$Br\zeta_{,r} \cot \theta + (2 - B)\zeta_{,\theta} = 2Br \nu_{,r} \nu_{,\theta} + 2(1 - B)\cot \theta - \frac{1}{2} B^3 r^3 e^{-4\nu} \omega_{,r} \omega_{,\theta} \sin^2 \theta. \tag{15}$$

2.1. Counter-rotating Interpretation of Thin Disks

When asking about the counterbalance to its (and the black hole's) gravity, the disk may either be considered as a solid structure (a set of circular hoops) or, on the contrary, as a non-coherent mix of azimuthal streams. In the astrophysical context, one usually adheres to the latter extreme possibility: that the disk is composed of two non-interacting streams of particles that follow stationary circular orbits in opposite azimuthal directions (Morgan & Morgan 1969; Lynden-Bell & Pineault 1978; Lamberti & Hamity 1989; Bičák et al. 1993; Bičák & Ledvinka 1993; Klein & Richter 1999; González & Espitia 2003; García-Reyes & González 2004). These orbits are geodesic if there is no radial stress acting within the disk ($T^\rho_\rho = 0$). The surface energy-momentum tensor is thus decomposed as

$$S^{\alpha\beta} = \sigma_+ u_+^\alpha u_+^\beta + \sigma_- u_-^\alpha u_-^\beta, \tag{16}$$

where the $+/-$ signs indicate the stream orbiting in a positive/negative sense of ϕ, taken with respect to the "average" fluid four-velocity u^α. The four-velocities are of the $u_\pm^\alpha = u_\pm^\alpha(1, 0, 0, \Omega_\pm)$ form again, so

$$S_\phi^t = B\rho e^{-2\nu}\left(\frac{\sigma_+ v_+}{1 - v_+^2} + \frac{\sigma_- v_-}{1 - v_-^2}\right), \quad S_\phi^\phi - \omega S_\phi^t = \frac{\sigma_+ v_+^2}{1 - v_+^2} + \frac{\sigma_- v_-^2}{1 - v_-^2}, \quad -S_t^t - \omega S_\phi^t = \frac{\sigma_+}{1 - v_+^2} + \frac{\sigma_-}{1 - v_-^2}, \tag{17}$$

now with $\Omega_\pm$ (and the corresponding $v_\pm$) given by free circular motion, i.e., by the roots of the equation $g_{tt,\alpha} + 2g_{t\phi,\alpha}\Omega + g_{\phi\phi,\alpha}\Omega^2 = 0$. Such a motion is only possible in the equatorial plane ($z = 0$) in general, where just the radial component of acceleration remains relevant, vanishing if

$$\Omega = \Omega_\pm = \omega + \frac{g_{\phi\phi}\omega_{,\rho}}{g_{\phi\phi,\rho}} \pm \sqrt{\left(\omega + \frac{g_{\phi\phi}\omega_{,\rho}}{g_{\phi\phi,\rho}}\right)^2 - \frac{g_{tt,\rho}}{g_{\phi\phi,\rho}}} \, ; \tag{18}$$

in particular, with the $B = 1$ choice, this expression reduces to

$$\Omega_\pm = \omega + \frac{\rho^2 \omega_{,\rho} \pm \sqrt{(\rho^2 \omega_{,\rho})^2 + 4e^{4\nu}\rho\nu_{,\rho}(1 - \rho\nu_{,\rho})}}{2\rho(1 - \rho\nu_{,\rho})}. \tag{19}$$

The interpretation is only possible when the expression under the square root is non-negative; physically, this is not satisfied for disks with "too much matter on larger radii": in such a case, the total gravitational pull at a given location points *outwards*, so "no angular velocity is low enough" to admit Keplerian orbiting there. Parameters of the counter-rotating picture ($\sigma_\pm, \Omega_\pm$) and the "total," one-stream parameters (σ, P, Ω) are related by comparing the two respective forms of the energy-momentum tensor, $\sigma u^\alpha u^\beta + P w^\alpha w^\beta = \sigma_+ u_+^\alpha u_+^\beta + \sigma_- u_-^\alpha u_-^\beta$. From the trace of this equation and from its projections onto $u_\alpha u_\beta$ and $w_\alpha w_\beta$, while using a suitable expression of the scalar products

$$u_\pm^\alpha u_\alpha = \frac{vv_\pm - 1}{\sqrt{1 - v^2}\sqrt{1 - v_\pm^2}}, \quad u_\pm^\alpha w_\alpha = \frac{v_\pm - v}{\sqrt{1 - v^2}\sqrt{1 - v_\pm^2}}, \quad g_{\alpha\beta} u_+^\alpha u_-^\beta = \frac{v_+ v_- - 1}{\sqrt{1 - v_+^2}\sqrt{1 - v_-^2}}, \tag{20}$$

one finds

$$\sigma - P = \sigma_+ + \sigma_-, \quad \sigma = \frac{\sigma_+(vv_+ - 1)^2}{(1 - v^2)(1 - v_+^2)} + \frac{\sigma_-(vv_- - 1)^2}{(1 - v^2)(1 - v_-^2)}, \quad P = \frac{\sigma_+(v_+ - v)^2}{(1 - v^2)(1 - v_+^2)} + \frac{\sigma_-(v_- - v)^2}{(1 - v^2)(1 - v_-^2)}, \tag{21}$$

$$\frac{P}{\sigma} = \frac{u_+^\alpha w_\alpha}{u_+^\beta u_\beta} \frac{u_-^\lambda w_\lambda}{u_-^\kappa u_\kappa} = \frac{(v_+ - v)(v - v_-)}{(1 - vv_+)(1 - vv_-)} \quad \Longrightarrow \quad \frac{\sigma + P}{\sigma_+ + \sigma_-} = \frac{1 + \frac{P}{\sigma}}{1 - \frac{P}{\sigma}} = ..., \tag{22}$$

$$\sigma_\pm (u_\pm^t)^2 = \pm \frac{S^{t\phi} - \Omega_\pm S^{tt}}{\Omega_+ - \Omega_-} \quad \Longrightarrow \quad \frac{\sigma_\pm}{1 - v_\pm^2} = \pm \frac{\sigma(v_\pm - v) - Pv(1 - vv_\pm)}{(1 - v^2)(v_+ - v_-)}. \tag{23}$$

We may also, for example, compare expressions for $S_{\alpha\beta}S^{\alpha\beta}$, finding the relation

$$\sigma^2 + P^2 = \sigma_+^2 + \sigma_-^2 + 2\sigma_+\sigma_-(g_{\alpha\beta}u_+^\alpha u_-^\beta)^2 = \sigma_+^2 + \sigma_-^2 + 2\sigma_+\sigma_- \frac{(1 - v_+v_-)^2}{(1 - v_+^2)(1 - v_-^2)}, \tag{24}$$

which in combination with $\sigma - P = \sigma_+ + \sigma_-$ also leads to

$$\sigma P = \sigma_+\sigma_- \frac{(v_+ - v_-)^2}{(1 - v_+^2)(1 - v_-^2)}, \quad (\sigma_+ - \sigma_-)^2 = (\sigma + P)^2 - 4\sigma P \frac{(1 - v_+v_-)^2}{(v_+ - v_-)^2}. \tag{25}$$

2.2. One-stream and Two-stream Interpretations: Integrating Jumps in the Field Equations

Relation between the jumps of $g_{\alpha\beta,\mu}$ across the disk and S_β^α are obtained by integrating the field Equations (5)–(8) over the infinitesimal interval $\langle z = 0^-, z = 0^+ \rangle$. Only the terms proportional to $\delta(z)$ (i.e., the source terms on the right-hand sides and the terms linear in $B_{,zz}$, $\nu_{,zz}$, $\omega_{,zz}$, and $\zeta_{,zz}$ on the left-hand side) contribute according to $\int_{z=0^-}^{z=0^+} \nu_{,zz} dz = 2\nu_{,z}(z = 0^+)$ (etc.), so we have $B_{,z}(z = 0^+) = 0$ and

$$\nu_{,z}(z = 0^+) = 2\pi(S_\phi^\phi - 2\omega S_\phi^t - S_t^t) = 2\pi(\sigma + P)\frac{1 + v^2}{1 - v^2} = 2\pi\left(\sigma_+ \frac{1 + v_+^2}{1 - v_+^2} + \sigma_- \frac{1 + v_-^2}{1 - v_-^2}\right), \tag{26}$$

$$\omega_{,z}(z = 0^+) = -\frac{8\pi S_\phi^t}{B^2\rho^2 e^{-4\nu}} = -8\pi(\sigma + P)\frac{\Omega - \omega}{1 - v^2} = -8\pi\left(\sigma_+ \frac{\Omega_+ - \omega}{1 - v_+^2} + \sigma_- \frac{\Omega_- - \omega}{1 - v_-^2}\right), \tag{27}$$

$$\zeta_{,z}(z = 0^+) = 4\pi(S_\phi^\phi - \omega S_\phi^t) = 4\pi \frac{\sigma v^2 + P}{1 - v^2} = 4\pi\left(\frac{\sigma_+ v_+^2}{1 - v_+^2} + \frac{\sigma_- v_-^2}{1 - v_-^2}\right), \tag{28}$$

where we have expressed the results in terms of the one-stream as well as the two-stream form of S_β^α.

3. Perturbation Scheme

We will look for a solution of Equations (6) and (7) in the form of series, expanding

$$\nu = \sum_{j=0}^\infty \nu_j \lambda^j, \quad \omega = \sum_{j=0}^\infty \omega_j \lambda^j, \quad \zeta = \sum_{j=0}^\infty \zeta_j \lambda^j, \tag{29}$$

where the coefficients ν_j, ω_j, and ζ_j depend on r and θ (or ρ and z), and the dimensionless parameter λ is proportional to the ratio of the disk mass to the black hole mass M, and more specifically, they are related by

$$(\sigma + P)\delta(z) \equiv \lambda\Sigma(\rho)\delta(z) = \lambda\Sigma(r)\frac{1}{r}\delta(\cos\theta) = -\lambda\Sigma(r)\frac{1}{r}\delta(\theta - \pi/2), \tag{30}$$

where δ denotes the δ-distribution and $\lambda\Sigma \equiv \sigma + P$ is an "effective" surface density. The functions ν_0, ω_0, and ζ_0 represent the black hole background, i.e., the Schwarzschild metric which in isotropic coordinates (recall that $\rho = r\sin\theta$ and $z = r\cos\theta$) reads

$$ds^2 = -\left(\frac{2r - M}{2r + M}\right)^2 dt^2 + \left(1 + \frac{M}{2r}\right)^4 (dr^2 + r^2 d\theta^2 + r^2 \sin^2\theta \, d\phi^2), \tag{31}$$

hence

$$\nu_0 = \ln\frac{2r - M}{2r + M}, \quad \omega_0 = 0, \quad B = e^{\zeta_0} = 1 - \frac{M^2}{4r^2}, \tag{32}$$

and the corresponding orbital velocity is

$$\Omega_0 = \frac{8\sqrt{Mr^3}}{(2r+M)^3}, \quad v_0 = \frac{2\sqrt{Mr}}{2r-M}. \tag{33}$$

Substituting Equations (29) and (30) into Equations (6) and (7), and subtracting the pure Schwarzschild terms, one obtains

$$\sum_{k=1}^{\infty} \lambda^k \nabla \cdot (B\nabla \nu_k) = \sum_{k=2}^{\infty} \lambda^k \left\{ \frac{(2r+M)^7 \sin^2\theta}{2^7 r^4 (2r-M)} \sum_{l=0}^{k-2} \left[\exp\left(-4\sum_{j=1}^{\infty} \lambda^j \nu_j\right) \right]_l \sum_{m=1}^{k-l-1} \nabla \omega_m \cdot \nabla \omega_{k-l-m} \right\}$$
$$+ 4\pi \frac{B}{r} \Sigma \, \delta(\cos\theta) \sum_{k=0}^{\infty} \lambda^{k+1} \left[\frac{1+v^2}{1-v^2} \right]_k, \tag{34}$$

$$\sum_{k=1}^{\infty} \lambda^k \nabla \cdot \left\{ \frac{(2r+M)^7 \sin^2\theta}{2^6 r^4 (2r-M)} \nabla \omega_k \right\} = -\sum_{k=2}^{\infty} \lambda^k \sum_{l=1}^{k-1} \nabla \cdot \left\{ \frac{(2r+M)^7 \sin^2\theta}{2^6 r^4 (2r-M)} \left[\exp\left(-4\sum_{j=1}^{\infty} \lambda^j \nu_j\right) \right]_{k-l} \nabla \omega_l \right\}$$
$$- 16\pi \left(1 + \frac{M}{2r} \right)^4 \Sigma \, \delta(\cos\theta) \sum_{k=0}^{\infty} \lambda^{k+1} \left[\frac{v}{1-v^2} \right]_k, \tag{35}$$

where $[f]_k$ means the coefficient standing at λ^k in a Taylor expansion of f. Since the background is static, the first-order equations only contain the mass–energy terms multiplied by the background metric on the right-hand sides, because the first-line sums do not contribute. In higher orders, the right-hand sides contain only lower-order terms. (For non-static backgrounds, the equations do not decouple as easily.)

Now, the eigenfunctions with respect to θ of the operator on the left-hand sides of Equations (34) and (35) are the Legendre polynomials $P_l(\cos\theta)$ and the Gegenbauer polynomials $C_l^{(3/2)}(\cos\theta)$, respectively.[5] Introducing a dimensionless radius $x := \frac{r}{M}\left(1 + \frac{M^2}{4r^2}\right)$, we may thus write

$$\nu_l = \sum_{j=0}^{\infty} \nu_{lj}(x) P_j(\cos\theta), \quad \omega_l = \sum_{j=0}^{\infty} \omega_{lj}(x) C_j^{(3/2)}(\cos\theta). \tag{36}$$

Substituting this into Equations (34) and (35) leads to

$$\sum_{j=0}^{\infty} \left\{ \frac{d}{dx}\left[(x^2-1)\frac{d\nu_{lj}}{dx} \right] - j(j+1)\nu_{lj} \right\} P_j(\cos\theta) = R_l(x, \theta), \tag{37}$$

$$\sum_{j=0}^{\infty} \left\{ (x^2-1)\frac{d}{dx}\left[(x+1)^4 \frac{d\omega_{lj}}{dx} \right] - (x+1)^4 j(j+3)\omega_{lj} \right\} C_j^{(3/2)}(\cos\theta) = S_l(x, \theta), \tag{38}$$

where $R_l(x, \theta)$ and $S_l(x, \theta)$ stand, up to an l-independent multiplication factor, for the coefficients of expansion (with respect to λ) of the right-hand sides of Equations (34) and (35); specifically,

$$\sum_{l=0}^{\infty} R_l(x, \theta)\lambda^l = \frac{r^2}{B}[\text{r.h.s. of (34)}], \quad \sum_{l=0}^{\infty} S_l(x, \theta)\lambda^l = \frac{Br^4}{M^4 \sin^2\theta}[\text{r.h.s. of (35)}]. \tag{39}$$

Provided that R_l and S_l do not diverge on the axis $\theta = 0, \pi$, these coefficients can also be decomposed as

$$R_l(x, \theta) = \sum_{j=0}^{\infty} R_{lj}(x) P_j(\cos\theta), \quad S_l(x, \theta) = \sum_{j=0}^{\infty} S_{lj}(x) C_j^{(3/2)}(\cos\theta), \tag{40}$$

where

$$R_{lj}(x) = \frac{2j+1}{2} \int_{-1}^{1} R_l(x, \theta) P_j(\cos\theta)\, d(\cos\theta), \tag{41}$$

$$S_{lj}(x) = \frac{2j+3}{2(j+1)(j+2)} \int_{-1}^{1} S_l(x, \theta) C_j^{(3/2)}(\cos\theta) \sin^2\theta \, d(\cos\theta). \tag{42}$$

---

[5] In Will's article, the latter are denoted by $T_l^{3/2}(\cos\theta)$.

Demanding that Equations (37) and (38) hold for each order (multipole moment) separately, one obtains a system of independent ordinary differential equations:

$$\frac{d}{dx}\left[(x^2 - 1)\frac{d\nu_{lj}}{dx}\right] - j(j + 1)\nu_{lj} = R_{lj}, \tag{43}$$

$$(x^2 - 1)\frac{d}{dx}\left[(x + 1)^4\frac{d\omega_{lj}}{dx}\right] - (x + 1)^4 j(j + 3)\omega_{lj} = S_{lj}, \tag{44}$$

where $l \in \mathbb{N}$, $j \in \mathbb{Z}_0^+$. They only contain lower-order source terms (assumed to be given) for every l and are to be supplemented by boundary conditions on the horizon $x = 1$ (ν_{lj} and ω_{lj} are supposed to be regular there) and at spatial infinity (ν_{lj} and ω_{lj} should vanish there). Of the many techniques available for such equations, we shall focus on finding their Green's functions.

Let us start from the fundamental systems of Equations (43) and (44). The first one is the Legendre differential equation whose fundamental system can be expressed as a linear combination of Legendre functions of the first and second kinds:

$$P_j(x) \quad \text{and} \quad Q_j(x) = P_j(x)\int_x^\infty \frac{d\xi}{(\xi^2 - 1)[P_j(\xi)]^2}. \tag{45}$$

For the second equation, Will (1974) used the substitution $t = (x + 1)/2$ which transforms it to the hypergeometric differential equation, having two generators of the fundamental system,

$$F_j(x) = {}_2F_1\left(-j, j + 3; 4; \frac{x + 1}{2}\right) \text{ and } G_j(x) = F_j(x)\int_x^\infty \frac{d\xi}{(\xi + 1)^4[F_j(\xi)]^2}, \tag{46}$$

where ${}_2F_1(a, b; c; \xi)$ denotes the Gauss hypergeometric function. Note that since $j \in \mathbb{Z}_0^+$, $F(x)$ is in fact a polynomial of degree j. Asymptotically (as $x \to \infty$), $P_j(x) \sim x^j$, $Q_j(x) \sim x^{-l-1}$, $F(x) \sim x^j$, and $G(x) \sim x^{-j-3}$. At the horizon ($x = 1$), $Q_j(x)$ and $G_j(x)$ diverge (except $G_0(x)$, which will be discussed later).

Given the above boundary conditions, the Green's functions of Equations (37) and (38) can be found in the form

$$\mathcal{G}_j^\nu(x, x') = \begin{cases} -Q_j(x)P_j(x') & \text{for } x \geqslant x' \\ -P_j(x)Q_j(x') & \text{for } x \leqslant x' \end{cases}, \tag{47}$$

$$\mathcal{G}_j^\omega(x, x') = \begin{cases} -G_j(x)F_j(x') & \text{for } x \geqslant x' \\ -F_j(x)G_j(x') & \text{for } x \leqslant x' \end{cases}, \tag{48}$$

and their inhomogeneous solutions as

$$\nu_{lj}(x) = \int_1^\infty R_{lj}(x')\mathcal{G}_j^\nu(x, x')\,dx', \tag{49}$$

$$\omega_{lj}(x) = \int_1^\infty S_{lj}(x')\mathcal{G}_j^\omega(x, x')\,dx' + \frac{J_l\,\delta_j^0}{(x + 1)^3}, \tag{50}$$

where J_l are arbitrary constants, representing a choice of the black hole spin (see Section 3.1). Such a solution is unique up to a coordinate transformation. Note that one could add to the Green functions terms proportional to $P_0(x) = F_0(x) = 1$ which is everywhere finite, but such an addition only corresponds to a rescaling of time and (thus) of the coordinate angular velocity, so it has no invariant physical effect.

Using Equation (36), we may write

$$\nu_l(x, \theta) = \sum_{j=0}^\infty \nu_{lj}(x)P_j(\cos\theta) = \int_1^\infty \sum_{j=0}^\infty R_{lj}(x')\mathcal{G}_j^\nu(x, x')P_j(\cos\theta)\,dx'$$
$$= \int_1^\infty \int_{-1}^1 R_l(x', \theta')\mathcal{G}^\nu(x, \theta, x', \theta')\,dx'\,d(\cos\theta'), \tag{51}$$

$$\omega_l(x, \theta) = \sum_{j=0}^\infty \omega_{lj}(x)C_j^{(3/2)}(\cos\theta) = \int_1^\infty \sum_{j=0}^\infty S_{lj}(x')\mathcal{G}_j^\omega(x, x')C_j^{(3/2)}(\cos\theta)\,dx'$$
$$= \int_1^\infty \int_{-1}^1 S_l(x', \theta')\mathcal{G}^\omega(x, \theta, x', \theta')\,dx'\,d(\cos\theta'), \tag{52}$$

where

$$\mathcal{G}^\nu(x, \theta, x', \theta') := -\sum_{j=0}^{\infty} \frac{2j+1}{2} P_j(\min(x, x')) Q_j(\max(x, x')) P_j(\cos\theta) P_j(\cos\theta'), \tag{53}$$

$$\mathcal{G}^\omega(x, \theta, x', \theta') := -\sum_{j=0}^{\infty} \frac{2j+3}{2(j+1)(j+2)} F_j(\min(x, x')) G_j(\max(x, x')) C_j^{(3/2)}(\cos\theta) C_j^{(3/2)}(\cos\theta') \left[+\frac{J_l}{(x+1)^3}\right] \tag{54}$$

are the Green's functions of the homogeneous parts of Equations (34) and (35). These represent a perturbation by an infinitesimal (2D) circular ring placed at x', θ' in the first order in λ. (We omit the J_l term in the following; see below.)

3.1. Differences from Will's Article

Will (1974) found the Green's functions of Equations (47) and (48) or, more precisely, he proposed the inhomogeneous solutions, Equations (49) and (50). He employed *three* expansions of the solutions: with respect to the linear mass density of the ring, with respect to the angular velocity of the horizon, and the multipole expansion performed to convert partial differential equations into ordinary ones. In contrast, we use only *two* expansions: with respect to the disk density and the multipole expansion. Below (see Section 5), we will even be able to drop the multipole expansion and work solely with the expansion with respect to the disk (ring) density. Namely, the rotational expansion can be "reconstructed" using the constants J_l (not employed in Will's paper). This is possible due to $F_j(1) = 0$ for $j > 0$ (see, for example, Equation (67)), which implies that higher multipole moments do not contribute to the black hole angular velocity at all, with the only important entering terms (in a given order λ^l of the mass perturbation) being proportional to $F_0(x) = 1$, $G_0(x) = (x+1)^{-3}$, or $\omega_{l0}(x)$, where ω_{l0} is the inhomogeneous solution of Equation (44) given by Equation (50) (with $J_l = 0$). The first term $F_0(x) = 1$ only adds a constant coordinate angular velocity, so it is not a physical degree of freedom (it can be cancelled out by a coordinate transformation). The meaning of the remaining two terms is revealed by their behavior in the vicinity of the disk (ring): G_0 is smooth everywhere, but ω_{l0} jumps in its first derivative (in the disk case, it thus contributes to the density of the disk energy-momentum). Hence, the term proportional to G_0 can be interpreted as the black hole's "own" angular velocity (perturbation toward the Kerr solution), while the terms proportional to ω_{l0} represent rotational perturbation due to the presence of the rotating disk (ring). Needless to say, such an interpretation is not unique, because $\omega_{l0} + C_l G_0$ (C_l are arbitrary constants) is also a solution of Equation (44) contributing to the source. Since there is no clear way to say which choice of C_l is the "correct" one, we will adhere to $C_l = 0$ for simplicity.

Having prescribed the black hole angular velocity

$$\omega_{\mathrm{H}} = \sum_{l=1}^{\infty} \beta_l \lambda^l, \tag{55}$$

one can find the J_l constants according to

$$J_l = 8[\beta_l - \omega_{l0}(1)|_{J_l=0}] = 8\beta_l + \int_1^{\infty} \frac{8S_{l0}(x')}{(x'+1)^3} \, dx', \tag{56}$$

where $\omega_{lj}|_{J_l=0}$ stands for the right-hand side of Equation (50) with $J_l = 0$, and S_{l0} contains lower-order terms of the expansion in λ (i.e., it also contains J_k with $k < l$).

4. Convergence and Related Issues

The main attribute of the above procedure is its speed of convergence to the desired solution. The problem is familiar from spectral methods (multipole expansion can actually be viewed as a spectral method): the numerics works well when the desired result is smooth; otherwise, convergence problems arise. More specifically, one can expect exponential convergence for the analytical function, whereas at most a power-law one can be expected for functions having some of their derivatives discontinuous (see, for example, Grandclément & Novak 2008).

Let us begin with the potential for the ring case. Focusing on the region *outside* the black hole, $1 \leqslant x_< \leqslant x_>$, and regarding the asymptotic behavior of special functions (see, for example, Olver et al. 2010), one can, after lengthy calculations, find that

$$\frac{2j+1}{2} P_j(\cos\theta) P_j(x_<) Q_j(x_>) P_j(0) \approx \frac{1}{j} \left(\frac{x_< + \sqrt{x_<^2 - 1}}{x_> + \sqrt{x_>^2 - 1}}\right)^{\frac{1}{2}+j} [f(x, x') + O(1/j)], \tag{57}$$

where $f(x, x')$ is a suitable function independent of j, $x_< := \min(x, x')$ and $x_> := \max(x, x')$. This implies that the sum (51) exponentially converges outside the ring radius and *conditionally* converges (like $1/j$) just on the radius of the ring. Practically, this means that near the ring radius, one has to include quite many terms (in j) in order to get reasonably small oscillations. (Convergence could be expected to be slow near a singular source.)

In the disk case, the situation is better and worse at the same time. After a lengthy calculation again, one finds that

$$\left| \int_{x_{R-}}^{x_{R+}} \frac{2j+1}{2} R_l(x_R) P_j(\cos\theta) P_j(x_<) Q_j(x_>) P_j(0)\, dx_R \right| < \frac{1}{j^2}\left(\frac{x'_< + \sqrt{x'^2_< - 1}}{x'_> + \sqrt{x'^2_> - 1}} \right)^{\frac{1}{2}+j} [f(x, x') + O(1/j)], \tag{58}$$

where $x_<$ and $x_>$ have the same meaning as above, i.e., $x_< := \min(x, x_R)$ and $x_> := \max(x, x_R)$, and $x'_<$, $x'_>$ stand for analogous quantities taken with respect to the nearest radius lying inside the disk (x'_R), i.e.,

$$x'_< = \begin{cases} x & \text{when} \quad x \leqslant x_{out} \\ x_{out} & \text{when} \quad x \geqslant x_{out} \end{cases}, \quad x'_> = \begin{cases} x_{in} & \text{when} \quad x \leqslant x_{in} \\ x & \text{when} \quad x \geqslant x_{in} \end{cases}, \tag{59}$$

where x_{in} and x_{out} represent inner and outer rims of the disk.

Equation (58) factually yields a lower bound of the convergence speed. (One can already obtain a speed estimate by checking the simplest example, i.e., constant S_{lj}.) We can thus conclude that in the disk case, convergence is exponentially fast at radii outside the disk and polynomial (like j^{-2}) at radii "within" the disk. Therefore, it is generally impossible to improve the polynomial convergence by using interpolation in some infinitesimally small area.

Calculation of dragging (ω_{jl}) shows a similar behavior, i.e., exponential convergence at radii outside of the ring (disk) and polynomial, like j^{-1} (j^{-2}), at the radii of the source. It is somewhat longer to prove this, so let us only say that one can proceed as follows: (i) prove that $dD_n^{(\gamma)}(x)/dx = -2\gamma\, D_{n-1}^{(\gamma+1)}(x)$, where $D_n^{(\gamma)}(x)$ is the second independent solution of the ultraspherical differential equation (the "second Gegenbauer function"; see Section 5 below), (ii) express $F_j(x)$ and $G_j(x)$ using Equation (67), and (iii) consider the asymptotic behavior of the Gegenbauer functions.

There is one more challenge for numerical precision: the integrals (45) and (46), when expressed using elementary functions, have the form of two terms almost cancelling each other. This problem can be managed by recalling that the Legendre function of the second kind $Q_j(x)$ can be expressed in terms of elementary functions and then evaluated efficiently. Analogously, $G_j(x)$ can be expressed as

$$G_j(x) = \frac{(-1)^j (j+2)!(j+3)!}{48(2j+3)!}\left(\frac{2}{x+1} \right)^{j+3} {}_2F_1\left(j, j+3; 2j+4; \frac{2}{x+1} \right), \tag{60}$$

which converges very well after the Gauss hypergeometric function is expanded suitably. Let us add that we do not know how to prove the equivalence of Equations (60) and (46) *directly*. However, it is possible to check that both expressions of $G_j(x)$ solve the homogeneous part of Equation (44) and that both vanish at $x \to \infty$. Equation (44) is a second-order ordinary linear differential equation, so its fundamental space is two dimensional. And since the other solution $F_j(x)$ does not vanish at infinity, both expressions of $G_j(x)$ have to be proportional to each other. Comparing their leading terms (of expansion in $1/x$), one finally concludes that the functions exactly coincide.

5. Green's Functions

To overcome the convergence problems, one can try to avoid angular expansion. A straightforward way to do so is to express the Green's functions $\mathcal{G}^\nu(x, \theta, x', \theta')$ and $\mathcal{G}^\omega(x, \theta, x', \theta')$ in closed form. This section is devoted to this task and uses relations that we will justify in detail elsewhere (P. Čížek 2017, in preparation). As an advertisement for the use of the closed-form Green's functions, see Figure 1, where, in an example of ring perturbation, the results are computed (i) by the usual expansions and (ii) using the closed-form Green's functions. The first 30 terms of the multipole expansion are summed there, but the closed-form Green's functions provide better results. See also Tables 1 and 2, where the convergence of the multipole expansion toward the exact result (given by the closed-form Green's functions) is illustrated. One should admit that the multipole series of this type can usually be re-summed in such a way that their convergence is much better even close to the source radius. Anyway, the main advantage of the closed-form Green's functions is that one can better integrate them over the source, as exemplified in Section 6 below.

5.1. Green's Function for the Gravitational Potential

In order to find the closed form of the Green's function (53), one can start from a more general relation, which will be proven in an accompanying paper by P. Čížek (2017, in preparation):[6]

$$\sum_{j=0}^{\infty} 2(j+\gamma) \frac{\Gamma^3(j+1)}{\Gamma^3(j+2\gamma)}\, D_j^{(\gamma)}(a) C_j^{(\gamma)}(u) C_j^{(\gamma)}(v) C_j^{(\gamma)}(w)$$

$$= \frac{\pi \int_{vw-\sqrt{(1-v^2)(1-w^2)}}^{vw+\sqrt{(1-v^2)(1-w^2)}} {}_2F_1\left(\frac{1}{2}, 1; \gamma+\frac{1}{2}; \frac{(1-u^2)(1-\xi^2)}{(a-u\xi)^2} \right) \frac{(1-v^2-w^2-\xi^2+2vw\xi)^{\gamma-1}}{a-u\xi}\, d\xi}{2^{4\gamma-2}\Gamma^4(\gamma)\Gamma(2\gamma)[(a^2-1)(1-v^2)(1-w^2)]^{\gamma-\frac{1}{2}}}, \tag{61}$$

---

[6] It is also shown there that the presented sum converges absolutely when $\gamma = 3/2$.
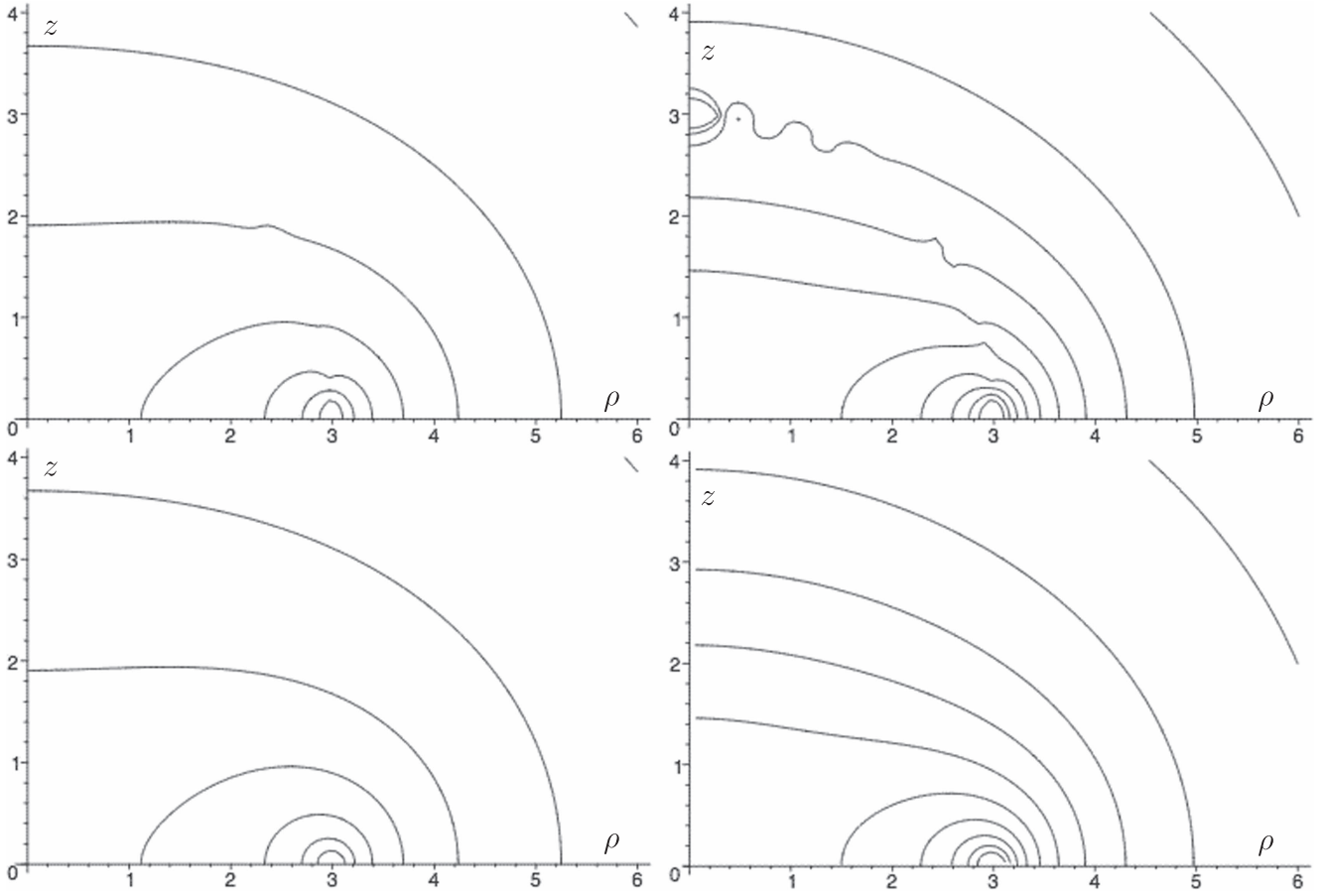
Figure 1. Meridional-plane contours of the gravitational potential (ν_1; left column) and of the linear dragging term (ω_1; right column), generated by a thin ring of matter located at $r = 3\mathcal{M}$ and having rest mass $0.01\mathcal{M}$ (where $\mathcal{M}$ is some mass scale; note that here the disk is the only source, there is no black hole). In the first row, the metric functions are calculated by summing the first 30 orders of multipole expansion, yet there are still obvious problems near the ring radius. In the second row, the same are computed (with a clearly better accuracy) using the closed-form Green's functions derived in Section 5. The coordinate axes are given in units of M.

where u, v, $w \in (-1; 1)$, a should be greater than 1, and $C_j^{(\gamma)}(x)$ and $D_j^{(\gamma)}(x)$ denote, respectively, Gegenbauer functions of the first and second kinds. Namely, $C_j^{(\gamma)}(x)$ and $D_j^{(\gamma)}(x)$ are two independent solutions of the ultraspherical differential equation

$$(1 - x^2)\frac{d^2 y(x)}{dx^2} - (2\gamma + 1)x\,\frac{dy(x)}{dx} + j(j + 2\gamma)y(x) = 0. \tag{62}$$

The first solution can be written as

$$C_n^{(\gamma)}(x) = |1 - x^2|^{\frac{1-2\gamma}{4}} \frac{\sqrt{2\pi}\,\Gamma(n + 2\gamma)}{2^\gamma \Gamma(\gamma)\Gamma(n + 1)} \times \begin{cases} \mathrm{P}^{\frac{1}{2}-\gamma}_{-\frac{1}{2}+\gamma+n}(x) & \text{when } |x| < 1 \\[2mm] P^{\frac{1}{2}-\gamma}_{-\frac{1}{2}+\gamma+n}(x) & \text{when } x \geqslant 1 \end{cases}; \tag{63}$$

it reduces to Gegenbauer polynomials when n is a non-negative integer and to Legendre functions of the first kind (actually Legendre polynomials) for $\gamma = 1/2$. The second solution can be written analogously,

$$D_n^{(\gamma)}(x) = |1 - x^2|^{\frac{1-2\gamma}{4}} \frac{\sqrt{2\pi}\,\Gamma(n + 2\gamma)}{2^\gamma \Gamma(\gamma)\Gamma(n + 1)} \times \begin{cases} \mathrm{Q}^{\frac{1}{2}-\gamma}_{-\frac{1}{2}+\gamma+n}(x) & \text{when } |x| < 1 \\[2mm] e^{i\pi(\gamma-\frac{1}{2})}Q^{\frac{1}{2}-\gamma}_{-\frac{1}{2}+\gamma+n}(x) & \text{when } x \geqslant 1 \end{cases}; \tag{64}$$

it reduces to Legendre functions of the second kind for $\gamma = 1/2$ (hence our reason for calling it as such). Above, we have employed the notations $\mathrm{P}^\mu_\nu(x)$, $P^\mu_\nu(x)$, $\mathrm{Q}^\mu_\nu(x)$, and $Q^\mu_\nu(x)$ used in Olver et al. (2010), chapter 14, in order to distinguish the Ferrers functions of the first and second kinds (i.e., Legendre functions defined on the cut $|x| < 1$; written in roman) from the associated Legendre functions of the first and second kinds (defined on $x > 1$; written in italic).

Table 1
Convergence of the Multipole Expansion of the Green Function's for Gravitational Potential $\mathcal{G}^\nu$ Computed for a Ring with Radius $x' = 3$ Located in the Equatorial Plane ($\theta' = \pi/2$)

θ	x	Number of Terms Added in Equation (53)					Exact Value
		10	20	30	40	50	
$\pi/2$	2.00	−0.19807	−0.19813	−0.19813	−0.19813	−0.19813	−0.19813
	2.50	−0.22468	−0.22664	−0.22680	−0.22682	−0.22682	−0.22682
	2.90	−0.26750	−0.28772	−0.29629	−0.30058	−0.30293	−0.30636
	3.00	−0.28370	−0.31884	−0.34032	−0.35583	−0.36797	$-\infty$
	3.10	−0.25857	−0.27846	−0.28700	−0.29134	−0.29374	−0.29738
	3.50	−0.19552	−0.19818	−0.19849	−0.19853	−0.19854	−0.19854
	4.00	−0.15445	−0.15478	−0.15479	−0.15479	−0.15479	−0.15479
$\pi/3$	2.00	−0.17340	−0.17344	−0.17344	−0.17344	−0.17344	−0.17344
	2.50	−0.16688	−0.16747	−0.16754	−0.16755	−0.16755	−0.16755
	2.90	−0.15563	−0.15601	−0.15780	−0.15881	−0.15894	−0.15858
	3.00	−0.15196	−0.15038	−0.15329	−0.15671	−0.15813	−0.15585
	3.10	−0.15012	−0.15044	−0.15221	−0.15323	−0.15337	−0.15299
	3.50	−0.14007	−0.14071	−0.14085	−0.14086	−0.14086	−0.14086
	4.00	−0.12584	−0.12599	−0.12600	−0.12600	−0.12600	−0.12600
$\pi/4$	2.00	−0.16020	−0.16016	−0.16016	−0.16016	−0.16016	−0.16016
	2.50	−0.15061	−0.15003	−0.15008	−0.15008	−0.15008	−0.15008
	2.90	−0.14321	−0.13879	−0.14019	−0.14108	−0.14074	−0.14062
	3.00	−0.14178	−0.13419	−0.13694	−0.14025	−0.13889	−0.13816
	3.10	−0.13822	−0.13388	−0.13526	−0.13617	−0.13582	−0.13570
	3.50	−0.12655	−0.12582	−0.12591	−0.12592	−0.12592	−0.12592
	4.00	−0.11458	−0.11444	−0.11445	−0.11445	−0.11445	−0.11445
$\pi/6$	2.00	−0.15110	−0.15113	−0.15113	−0.15113	−0.15113	−0.15113
	2.50	−0.13920	−0.13971	−0.13975	−0.13974	−0.13974	−0.13974
	2.90	−0.12758	−0.12952	−0.13141	−0.13019	−0.13032	−0.13046
	3.00	−0.12402	−0.12610	−0.13108	−0.12705	−0.12729	−0.12817
	3.10	−0.12310	−0.12499	−0.12687	−0.12564	−0.12577	−0.12591
	3.50	−0.11656	−0.11716	−0.11722	−0.11721	−0.11721	−0.11721
	4.00	−0.10712	−0.10725	−0.10725	−0.10725	−0.10725	−0.10725
0	2.00	−0.14420	−0.14434	−0.14434	−0.14434	−0.14434	−0.14434
	2.50	−0.13010	−0.13270	−0.13242	−0.13246	−0.13245	−0.13245
	2.90	−0.10950	−0.13056	−0.11932	−0.12593	−0.12186	−0.12343
	3.00	−0.10054	−0.13646	−0.10871	−0.13221	−0.11144	−0.12127
	3.10	−0.10552	−0.12621	−0.11502	−0.12169	−0.11754	−0.11915
	3.50	−0.10822	−0.11153	−0.11104	−0.11112	−0.11111	−0.11111
	4.00	−0.10153	−0.10208	−0.10206	−0.10206	−0.10206	−0.10206

Note. Values at several latitudes θ are computed in the radial region close to the ring (from $x = 2$ to $x = 4$).

One more remark on the formula (61) is called for, namely, that it requires u to lie within $(-1; 1)$, while for a ring outside of the horizon, $u > 1$ actually. However, a function of a complex variable has a unique extension (up to a Riemann folding), so the solution is valid for $u \in (-1; 1)$ when extended into the complex plane, and should also yield a (unique) solution of the respective differential equations with different boundary conditions.

Relation (61) provides $\mathcal{G}^\nu(x, \theta, x', \theta')$ (up to a multiplication factor) if setting $\gamma = 1/2$, $a = \max(x, x')$, $u = \min(x, x')$, $v = \cos \theta$, and $w = \cos \theta'$. Namely, as will be shown in P. Čížek (2017, in preparation; the result follows from Baranov 2006),

$$\sum_{j=0}^{\infty} (2j+1) Q_j(a) P_j(u) P_j(v) P_j(w) = \frac{2 \, K\left[\sqrt{\frac{4\sqrt{(a^2-1)(u^2-1)(1-v^2)(1-w^2)}}{(au-vw)^2 - (\sqrt{(a^2-1)(u^2-1)} - \sqrt{(1-v^2)(1-w^2)})^2}}\right]}{\pi [(au-vw)^2 - (\sqrt{(a^2-1)(u^2-1)} - \sqrt{(1-v^2)(1-w^2)})^2]^{1/2}}, \tag{65}$$

hence, comparing this with Equation (53), we get

$$\mathcal{G}^\nu(x, \theta, x', \theta') = -\frac{K\left[\sqrt{\frac{4\sqrt{(x^2-1)(x'^2-1)}\sin\theta\sin\theta'}{(xx'-\cos\theta\cos\theta')^2 - (\sqrt{(x^2-1)(x'^2-1)} - \sin\theta\sin\theta')^2}}\right]}{\pi [(xx'-\cos\theta\cos\theta')^2 - (\sqrt{(x^2-1)(x'^2-1)} - \sin\theta\sin\theta')^2]^{1/2}}. \tag{66}$$

Table 2
Convergence of the Multipole Expansion of the Green's Function for Dragging $\mathcal{G}^\omega$ Computed for a Ring with Radius $x' = 3$ Located in the Equatorial Plane ($\theta' = \pi/2$)

θ	x	Number of Terms Added in Equation (54)					Exact Value
		10	20	30	40	50	
$\pi/2$	2.00	−0.0043591	−0.0043605	−0.0043605	−0.0043605	−0.0043605	−0.0043605
	2.50	−0.0050673	−0.0051175	−0.0051218	−0.0051222	−0.0051223	−0.0051223
	2.90	−0.0063084	−0.0068904	−0.0071424	−0.0072701	−0.0073402	−0.0074433
	3.00	−0.0067968	−0.0078323	−0.0084794	−0.0089513	−0.0093229	$-\infty$
	3.10	−0.0059006	−0.0064596	−0.0067049	−0.0068309	−0.0069010	−0.0070079
	3.50	−0.0037462	−0.0038087	−0.0038162	−0.0038173	−0.0038174	−0.0038175
	4.00	−0.0024485	−0.0024550	−0.0024551	−0.0024551	−0.0024551	−0.0024551
$\pi/3$	2.00	−0.0037082	−0.0037087	−0.0037087	−0.0037087	−0.0037087	−0.0037087
	2.50	−0.0033726	−0.0033758	−0.0033779	−0.0033781	−0.0033782	−0.0033781
	2.90	−0.0029896	−0.0029065	−0.0029373	−0.0029732	−0.0029866	−0.0029767
	3.00	−0.0029039	−0.0027174	−0.0027375	−0.0028423	−0.0029251	−0.0028643
	3.10	−0.0027625	−0.0026820	−0.0027111	−0.0027462	−0.0027598	−0.0027498
	3.50	−0.0022901	−0.0022911	−0.0022943	−0.0022948	−0.0022948	−0.0022948
	4.00	−0.0017923	−0.0017936	−0.0017938	−0.0017938	−0.0017938	−0.0017938
$\pi/4$	2.00	−0.0033785	−0.0033783	−0.0033783	−0.0033783	−0.0033783	−0.0033783
	2.50	−0.0029105	−0.0029114	−0.0029139	−0.0029139	−0.0029139	−0.0029139
	2.90	−0.0024557	−0.0024287	−0.0025224	−0.0025304	−0.0025057	−0.0025097
	3.00	−0.0023163	−0.0022347	−0.0024540	−0.0025018	−0.0023813	−0.0024098
	3.10	−0.0022598	−0.0022333	−0.0023241	−0.0023322	−0.0023075	−0.0023116
	3.50	−0.0019376	−0.0019385	−0.0019426	−0.0019426	−0.0019425	−0.0019425
	4.00	−0.0015499	−0.0015498	−0.0015500	−0.0015500	−0.0015500	−0.0015500
$\pi/6$	2.00	−0.0031638	−0.0031633	−0.0031633	−0.0031633	−0.0031633	−0.0031633
	2.50	−0.0026684	−0.0026508	−0.0026545	−0.0026543	−0.0026542	−0.0026543
	2.90	−0.0023803	−0.0021449	−0.0022923	−0.0022750	−0.0022750	−0.0022613
	3.00	−0.0023586	−0.0019140	−0.0022626	−0.0022328	−0.0020593	−0.0021686
	3.10	−0.0021926	−0.0019660	−0.0021091	−0.0020924	−0.0020616	−0.0020787
	3.50	−0.0017658	−0.0017434	−0.0017494	−0.0017490	−0.0017489	−0.0017490
	4.00	−0.0014080	−0.0014058	−0.0014060	−0.0014060	−0.0014060	−0.0014060
0	2.00	−0.0029876	−0.0030073	−0.0030070	−0.0030070	−0.0030070	−0.0030070
	2.50	−0.0020835	−0.0025531	−0.0024665	−0.0024810	−0.0024787	−0.0024790
	2.90	+0.0004811	−0.0045000	−0.0000854	−0.0037008	−0.0008545	−0.0020972
	3.00	+0.0019023	−0.0072430	+0.0042764	−0.0091957	+0.0059767	−0.0020094
	3.10	+0.0005373	−0.0042505	+0.0000482	−0.0035188	−0.0006733	−0.0019249
	3.50	−0.0011763	−0.0017360	−0.0015918	−0.0016257	−0.0016180	−0.0016194
	4.00	−0.0012397	−0.0013108	−0.0013062	−0.0013065	−0.0013064	−0.0013064

Note. Values at several latitudes θ are computed in the radial region close to the ring (from $x = 2$ to $x = 4$).

This is actually an expected result: the Green's function corresponds to the potential due to a thin-ring source (situated at x', θ'), which is known to be given by the complete elliptic integral $K(k)$ (within general relativity, such a source is known as the Bach-Weyl ring; see, e.g., Semerák 2016). Note in passing that Equation (6) is quadratic in dragging (ω) and the background metric is static (Schwarzschild solution), so the dragging has to be proportional to the perturbation (λ), i.e., the correction from the $(\nabla\omega)^2$ term is at least of order λ^2 and does not contribute in the linear order (in higher orders, it behaves like a source term). Without dragging, Equation (6) is the same as in the static case (or even a Newtonian one) and one reaches the above result (up to a coordinate transformation; see Equation (80)).

5.2. Green's Function for Dragging

Now we proceed to the second Green's function (54). Considering relations

$$F_j(x) = \frac{12(-1)^j}{j(j+1)^2(j+2)^2(j+3)} \hat{O}_x C_j^{(3/2)}(x), \quad G_j(x) = \frac{(-1)^j}{12} \hat{O}_x D_j^{(3/2)}(x), \tag{67}$$

$$\text{where} \quad \hat{O}_x := (x-1)\frac{d^2}{dx^2}(x-1) = \frac{d}{dx}(x-1)^2\frac{d}{dx}, \tag{68}$$

we can rewrite Equation (54) as

$$\mathcal{G}^\omega = \Delta - \sum_{j=1}^{\infty} \frac{j + \frac{3}{2}}{j(j+1)^3(j+2)^3(j+3)} \hat{O}_{x_<} C_j^{(3/2)}(x_<) \hat{O}_{x_>} D_j^{(3/2)}(x_>) C_j^{(3/2)}(\cos\theta) C_j^{(3/2)}(\cos\theta')$$

$$= \Delta - \hat{O}_{x_>} \frac{d}{dx_<}(x_< - 1)^2 \sum_{j=1}^{\infty} \frac{j + \frac{3}{2}}{j(j+1)^3(j+2)^3(j+3)} D_j^{(3/2)}(x_>) \frac{d}{dx_<} C_j^{(3/2)}(x_<) C_j^{(3/2)}(\cos\theta) C_j^{(3/2)}(\cos\theta')$$

$$= \widetilde{\Delta} - \hat{O}_{x_>} \frac{d}{dx_<}(x_< + 1)^{-2} \sum_{j=0}^{\infty} \frac{j + \frac{3}{2}}{(j+1)^3(j+2)^3} \int_1^{x_<} (\zeta^2 - 1) D_j^{(3/2)}(x_>) C_j^{(3/2)}(\zeta) C_j^{(3/2)}(\cos\theta) C_j^{(3/2)}(\cos\theta') \, d\zeta$$

$$= \widetilde{\Delta} - \hat{O}_{x_>} \frac{d}{dx_<} \int_1^{x_<} \frac{\zeta^2 - 1}{2(x_< + 1)^2} \sum_{j=0}^{\infty} \frac{2j + 3}{(j+1)^3(j+2)^3} D_j^{(3/2)}(x_>) C_j^{(3/2)}(\zeta) C_j^{(3/2)}(\cos\theta) C_j^{(3/2)}(\cos\theta') \, d\zeta$$

$$= \widetilde{\Delta} - \hat{O}_{x_>} \frac{d}{dx_<} \int_1^{x_<} \frac{\zeta^2 - 1}{2\pi(x_< + 1)^2(x_>^2 - 1)\sin^2\theta\sin^2\theta'} \int_{\cos(\theta+\theta')}^{\cos(\theta-\theta')} \frac{\sqrt{[\cos(\theta-\theta') - \xi][\xi - \cos(\theta+\theta')]}}{x_> - \zeta\xi + \sqrt{(x_> - \zeta\xi)^2 - (1-\zeta^2)(1-\xi^2)}} \, d\xi d\zeta, \quad (69)$$

where

$$\Delta := -\frac{3}{4} F_0(x_<) G_0(x_>) C_0^{(3/2)}(\cos\theta) C_0^{(3/2)}(\cos\theta') = -\frac{1}{4(x_> + 1)^3}, \quad (70)$$

$$\widetilde{\Delta} := \Delta + \hat{O}_{x_>} \frac{d}{dx_<} \frac{3}{16(x_< + 1)^2} \int_1^{x_<} (\zeta^2 - 1) D_0^{(3/2)}(x_>) C_0^{(3/2)}(\zeta) C_0^{(3/2)}(\cos\theta) C_0^{(3/2)}(\cos\theta') d\zeta$$

$$= -\frac{2}{(x + 1)^3(x' + 1)^3}. \quad (71)$$

We have deliberately switched the order of summation, integration, and differentiation, which might in fact be an issue, but we will later check that the result is really a Green's function of the original Equation (35) with the given boundary conditions. Note that the above result is simple, thanks to its symmetry with respect to $x_< \leftrightarrow x_>$, and also due to the relation

$$\int_1^x (z^2 - 1) C_n^{(3/2)}(z) \, dz = \frac{(x^2 - 1)^2}{n(n+3)} \frac{dC_n^{(3/2)}(x)}{dx}, \quad (72)$$

which is a direct consequence of the ultraspherical differential equation.

Calculation of the integral (69) leads to logarithms or elliptic functions, but, "miraculously," when one applies the operator $\hat{O}_{x_>}$ first and only then integrates by ζ, such difficulties do not occur, because

$$\frac{d}{dx_<} \int_1^{x_<} \hat{O}_{x_>} \frac{(\zeta^2 - 1) \, d\zeta}{2\pi(x_< + 1)^2(x_>^2 - 1)\sin^2\theta\sin^2\theta'[x_> - \zeta\xi + \sqrt{(x_> - \zeta\xi)^2 - (1-\zeta^2)(1-\xi^2)}]} = \sum_{k=0}^{5} \mathcal{P}_k(x', \theta') \tilde{I}_k(x', \xi), \quad (73)$$

where we have denoted

$$\mathcal{P}_0(x', \theta') := \frac{-2}{\pi(x+1)^3(x'+1)^3\sin^2\theta\sin^2\theta'}, \quad \tilde{I}_0(x', \xi) := 1,$$

$$\mathcal{P}_1(x', \theta') := \frac{-(x-1)(x'-1)}{\pi(x+1)^3(x'+1)^3\sin^2\theta\sin^2\theta'}, \quad \tilde{I}_1(x', \xi) := \frac{1}{\xi + 1},$$

$$\mathcal{P}_2(x', \theta') := \frac{2xx' + (x-1)(x'-1)}{\pi(x+1)^3(x'+1)^3\sin^2\theta\sin^2\theta'}, \quad \tilde{I}_2(x', \xi) := \frac{1}{\sqrt{x^2 + x'^2 + \xi^2 - 1 - 2xx'\xi}},$$

$$\mathcal{P}_3(x', \theta') := \frac{-2}{\pi(x+1)^3(x'+1)^3\sin^2\theta\sin^2\theta'}, \quad \tilde{I}_3(x', \xi) := \frac{\xi}{\sqrt{x^2 + x'^2 + \xi^2 - 1 - 2xx'\xi}},$$

$$\mathcal{P}_4(x', \theta') := \frac{(x'-1)(x-1)(x'+x)}{\pi(x+1)^3(x'+1)^3\sin^2\theta\sin^2\theta'}, \quad \tilde{I}_4(x', \xi) := \frac{1}{(\xi + 1)\sqrt{x^2 + x'^2 + \xi^2 - 1 - 2xx'\xi}},$$

$$\mathcal{P}_5(x', \theta') := \frac{(x-1)(x'-1)}{2\pi(x+1)(x'+1)\sin^2\theta\sin^2\theta'}, \quad \tilde{I}_5(x', \xi) := \frac{1}{(x^2 + x'^2 + \xi^2 - 1 - 2xx'\xi)^{3/2}}. \quad (74)$$

Therefore, we can finally conclude that

$$\mathcal{G}^\omega(x, \theta, x', \theta') = \widetilde{\Delta}(x, x') - \int_{\cos(\theta+\theta')}^{\cos(\theta-\theta')} \sqrt{[\cos(\theta - \theta') - \xi][\xi - \cos(\theta + \theta')]} \sum_{k=0}^{5} \mathcal{P}_k(x', \theta') \tilde{I}_k(x', \xi)\, d\xi$$

$$= \widetilde{\Delta}(x, x') - \sum_{k=0}^{5} \mathcal{P}_k(x', \theta') I_k(x', \theta'), \tag{75}$$

where

$$I_0(x', \theta') := \frac{\pi}{2} \sin^2\theta \sin^2\theta',$$

$$I_1(x', \theta') := \pi(1 - |\cos\theta|)(1 - |\cos\theta'|),$$

$$I_2(x', \theta') := \sqrt{\frac{a_{31}}{a_{42}}} \left[-a_{41}K(k) - a_{42}E(k) + a_{41}\left(1 + \frac{a_{42}}{a_{31}}\right)\Pi\left(-\frac{a_{43}}{a_{31}}, k\right) \right],$$

$$I_3(x', \theta') := \frac{a_{41}}{4} \sqrt{\frac{a_{31}}{a_{42}}} \left[-(s_{21} + s_{43} + 2a_{21})K(k) + \frac{a_{42}}{a_{41}}(s_{43} - 3s_{21})E(k) + \frac{a_{21}^2 - a_{43}^2 + 2s_{21}^2 - 2s_{21}s_{43}}{a_{31}} \Pi\left(-\frac{a_{43}}{a_{31}}, k\right) \right],$$

$$I_4(x', \theta') := \frac{2a_{41}}{\sqrt{a_{31}a_{42}}} \left[-\frac{K(k)}{a_1 + 1} + \Pi\left(-\frac{a_{43}}{a_{31}}, k\right) - \frac{a_3 + 1}{a_1 + 1} \Pi\left(-\frac{(a_1 + 1)a_{43}}{(a_4 + 1)a_{31}}, k\right) \right],$$

$$I_5(x', \theta') := \frac{2\sqrt{a_{31}a_{42}}}{a_{21}^2}[(2 - k^2)K(k) - 2E(k)], \tag{76}$$

with

$$a_1 := xx' + \sqrt{(x^2 - 1)(x'^2 - 1)}, \quad a_2 := xx' - \sqrt{(x^2 - 1)(x'^2 - 1)}, \quad a_3 := \cos(\theta - \theta'), \quad a_4 := \cos(\theta + \theta') \tag{77}$$

and

$$a_{rs} := a_s - a_r, \quad s_{rs} := a_s + a_r, \quad k := \sqrt{\frac{a_{21}a_{43}}{a_{31}a_{42}}}. \tag{78}$$

On the horizon, the above Green's function simplifies considerably,

$$\mathcal{G}^\omega(x = 1, \theta, x', \theta') = -\frac{1}{4(x' + 1)^3}. \tag{79}$$

Note that this is independent of the position on the horizon (i.e., of the angle θ), consistent with the well-known "rigid rotation" of stationary horizons.

6. Disk Solution

Perturbation equations can be solved by integrating the Green's functions over the source mass distribution. Due to the presence of (complete) elliptic integrals in the above concise expression of the Green's functions, numerical integration has to be employed in general. Integration is of course simpler for thin sources (surface distribution) than for extended ones. Below we consider the case of a stationary and axially symmetric thin disk, encircling the central black hole between some two finite radii $x_{\rm in} \leqslant x \equiv \frac{r}{M} + \frac{M}{4r} \leqslant x_{\rm out}$ in a concentric manner (thus lying in the equatorial plane). We will show how to obtain explicit results for the linear perturbation of the metric functions and for the corresponding basic characteristics (density, pressure, and velocity distribution) of the source.

6.1. Gravitational Potential

First, let us find the linear perturbation of the potential, ν_1. It is advantageous to choose $B = 1$ here, since this makes Equation (34) the Laplace/Poisson equation, so one can use its solutions known from classical field theory. Let us denote by $t, \phi, \tilde{\rho},$ and $\tilde{z}$ the coordinates corresponding to this choice (the time t and azimuth ϕ do not depend on the choice of B). Their counterparts (ρ, z) corresponding to $B = 1 - \frac{M^2}{4r^2}$ are related by

$$\tilde{\rho} = \frac{\rho(M^2 - 4\rho^2 - 4z^2)}{4(\rho^2 + z^2)} = \frac{(4r^2 - M^2)\sin\theta}{4r} = M\sqrt{x^2 - 1}\,\sin\theta,$$

$$\tilde{z} = \frac{z(M^2 + 4\rho^2 + 4z^2)}{4(\rho^2 + z^2)} = \frac{(4r^2 + M^2)\cos\theta}{4r} = Mx\cos\theta,$$

$$\tilde{\zeta} = \zeta - \frac{1}{2}\ln\left[\frac{(4\rho^2 + 4z^2 + M^2)^2 - 16M^2z^2}{16(\rho^2 + z^2)^2}\right] = \zeta - \frac{1}{2}\ln\left[\frac{(4r^2 + M^2)^2 - 16r^2M^2\cos^2\theta}{16r^4}\right] = \zeta - \frac{1}{2}\ln\frac{4(x^2 - \cos^2\theta)}{(x + \sqrt{x^2 - 1})^2} \tag{80}$$

(to recall the function ζ, we remind the reader that $g_{\rho\rho} = g_{rr} = e^{2\zeta-2\nu}$).

Of the known disk solutions of the Laplace equation, we will choose the one describing a disk that extends from the origin ($\tilde{\rho} = \tilde{z} = 0$) to some finite equatorial radius x' (or $\tilde{\rho}'$ when expressed in the Weyl radius corresponding to the $B = 1$ choice) and whose Newtonian surface density S is constant in the unperturbed $B = 1$ coordinate system. Such a solution was obtained by Lass & Blitzer ([1983](#)),

$$V(x'; x, \theta)$$

$$= 2\pi S|\tilde{z}|\, H(\tilde{\rho}' - \tilde{\rho}) - \frac{2S}{\sqrt{\tilde{z}^2 + (\tilde{\rho}' + \tilde{\rho})^2}}\left\{[\tilde{z}^2 + (\tilde{\rho}' + \tilde{\rho})^2]E(k) + (\tilde{\rho}'^2 - \tilde{\rho}^2)K(k) + \tilde{z}^2\,\frac{\tilde{\rho}' - \tilde{\rho}}{\tilde{\rho}' + \tilde{\rho}}\,\Pi\left[\frac{4\tilde{\rho}'\tilde{\rho}}{(\tilde{\rho}' + \tilde{\rho})^2}, k\right]\right\}$$

$$= 2\pi MSx|\cos\theta|\, H(x'^2 - \cos^2\theta - x^2\sin^2\theta)$$

$$- 2MS\,\frac{a_{31}a_{42}\,E(k) + (x'^2 - \cos^2\theta - x^2\sin^2\theta)K(k) + \frac{(a_{41}a_{32} - x^2\cos^2\theta)x^2\cos^2\theta}{x'^2 - \cos^2\theta - x^2\sin^2\theta}\,\Pi\left(\frac{2a_{21}\sin\theta}{a_{31}a_{42} - x^2\cos^2\theta}, k\right)}{\sqrt{a_{31}a_{42}}}, \tag{81}$$

where $H(x)$ stands for the Heaviside function, and the $a_{rs}(x')$ and $k(x')$ symbols are given by Equations ([77](#)) and ([78](#)) evaluated at $\theta' = \pi/2$,

$$a_1(x') = xx' + \sqrt{(x^2 - 1)(x'^2 - 1)},\quad a_2(x') = xx' - \sqrt{(x^2 - 1)(x'^2 - 1)},\ a_3(x') = \sin\theta,\quad a_4(x') = -\sin\theta,$$

$$a_{rs}(x') = a_s(x') - a_r(x'),\quad k^2(x') = \frac{2a_{21}\sin\theta}{a_{31}a_{42}} = \frac{4\sqrt{(x^2 - 1)(x'^2 - 1)}\,\sin\theta}{x^2x'^2 - [\sqrt{(x^2-1)(x'^2-1)} - \sin\theta]^2} = \frac{4\tilde{\rho}'\tilde{\rho}}{(\tilde{\rho}' + \tilde{\rho})^2 + \tilde{z}^2}. \tag{82}$$

The potential of a disk extending between two finite radii $x_{\text{in}} \leqslant x \leqslant x_{\text{out}}$ (which we are interested in) is obtained by the subtraction of two potentials ([81](#)) (with the same density S) with outer radii at x_{out} and x_{in},

$$\nu_1(x, \theta) = V(x' = x_{\text{out}}; x, \theta) - V(x' = x_{\text{in}}; x, \theta). \tag{83}$$

6.2. Dragging

In order to find the perturbation of the dragging angular velocity, one has to integrate Equation ([69](#)) over the "density" of the disk $W(x)$ (here assumed to be constant, W). Since, as already noted, Equation ([69](#)) is symmetric with respect to the exchange $x_< \leftrightarrow x_>$, we can substitute $x_<$ with x' and $x_>$ with x without changing the result:

$$\omega_1(x, \theta) = -\int_{x_{\text{in}}}^{x_{\text{out}}} W\,\mathcal{G}^\omega(x, \omega, x', \pi/2)dx'$$

$$= -\int_{x_{\text{in}}}^{x_{\text{out}}} W\,\widetilde{\Delta}(x, x')dx' + \int_{x_{\text{in}}}^{x_{\text{out}}} W\,\hat{O}_x\,\frac{d}{dx'}\int_1^{x'}\frac{\zeta^2 - 1}{\pi(x' + 1)^2\sin^2\theta(x^2 - 1)}\int_{-\sin\theta}^{\sin\theta}\frac{\sqrt{\sin^2\theta - \xi^2}\,d\xi\,d\zeta\,dx'}{x - \zeta\xi + \sqrt{(x - \zeta\xi)^2 - (1 - \zeta^2)(1 - \xi^2)}}$$

$$= \frac{(x_{\text{out}} - x_{\text{in}})(x_{\text{out}} + x_{\text{in}} + 2)W}{(x + 1)^3(x_{\text{in}} + 1)^2(x_{\text{out}} + 1)^2} + W\int_{-\sin\theta}^{\sin\theta}\left[\frac{\hat{O}_x}{2\pi\sin^2\theta}\int_1^{x'}\frac{\sqrt{\sin^2\theta - \xi^2}}{x - \zeta\xi + \sqrt{(x - \zeta\xi)^2 - (1 - \zeta^2)(1 - \xi^2)}}\frac{(\zeta^2 - 1)\,d\zeta}{(x' + 1)^2(x^2 - 1)}\right]_{x' = x_{\text{in}}}^{x_{\text{out}}}d\xi$$

$$= \frac{(x_{\text{out}} - x_{\text{in}})(x_{\text{out}} + x_{\text{in}} + 2)W}{(x + 1)^3(x_{\text{in}} + 1)^2(x_{\text{out}} + 1)^2} + W\int_{-\sin\theta}^{\sin\theta}\sqrt{\sin^2\theta - \xi^2}\sum_{j=0}^{7}[Q_j(x_{\text{out}})\tilde{I}_j(x_{\text{out}}, \xi) - Q_j(x_{\text{in}})\tilde{I}_j(x_{\text{in}}, \xi)]d\xi$$

$$= \frac{(x_{\text{out}} - x_{\text{in}})(x_{\text{out}} + x_{\text{in}} + 2)W}{(x + 1)^3(x_{\text{in}} + 1)^2(x_{\text{out}} + 1)^2} + W\sum_{j=0}^{7}[Q_j(x_{\text{out}}, \theta)I_j(x_{\text{out}}, \theta) - Q_j(x_{\text{in}}, \theta)I_j(x_{\text{in}}, \theta)], \tag{84}$$

where x_{in} and x_{out} mark, again, the inner and outer rims of the disk (in the coordinate x), $\tilde{I}_0, \ldots, \tilde{I}_5$ are defined by Equation ([74](#)),

$$\tilde{I}_6(x', \xi) = \frac{1}{\xi - 1},\quad \tilde{I}_7(x', \xi) = \frac{1}{(\xi - 1)\sqrt{x^2 + x'^2 + \xi^2 - 1 - 2xx'\xi}},$$

$$Q_0(x') = \frac{1}{\pi(x + 1)^3(x' + 1)^2\sin^2\theta},\quad Q_1(x') = \frac{(1 - x)(x' - 1)^2}{4\pi(x + 1)^3(x' + 1)^2\sin^2\theta},$$

$$Q_2(x') = \frac{x'(1 - 2x)}{\pi(x + 1)^3(x' + 1)^2\sin^2\theta},\quad Q_3(x') = \frac{1}{\pi(x + 1)^3(x' + 1)^2\sin^2\theta},$$

$$Q_4(x') = \frac{(x + x')(x - 1)(x' - 1)^2}{4\pi(x + 1)^3(x' + 1)^2\sin^2\theta},\quad Q_5(x') = 0,$$

$$Q_6(x') = \frac{(1 - x)}{4\pi(x + 1)^3\sin^2\theta},\quad Q_7(x') = \frac{(1 - x)(x' - x)}{4\pi(x + 1)^3\sin^2\theta}, \tag{85}$$

and $I_k(x')$ correspond to Equation (76) taken at $\theta' = \pi/2$,

$$I_0(x') = \frac{\pi}{2} \sin^2 \theta,$$

$$I_1(x') = \pi(1 - |\cos \theta|),$$

$$I_2(x') = \sqrt{\frac{a_{31}}{a_{42}}} \left[-a_{41}K(k) - a_{42}E(k) + 2xx' \frac{a_{41}}{a_{31}} \Pi\left(-\frac{2\sin\theta}{a_{31}}, k\right) \right],$$

$$I_3(x') = a_{41} \sqrt{\frac{a_{31}}{a_{42}}} \left[\frac{a_2 - 3a_1}{4} K(k) - \frac{3a_{42}}{2a_{41}} xx'E(k) + \frac{x^2 x'^2 + \cos^2\theta - (x - x')^2}{a_{31}} \Pi\left(-\frac{2\sin\theta}{a_{31}}, k\right) \right],$$

$$I_4(x') = \frac{2a_{41}}{\sqrt{a_{31}a_{42}}} \left\{ -\frac{a_{31}}{a_1 + 1} K(k) + \Pi\left(-\frac{2\sin\theta}{a_{31}}, k\right) - \frac{1 + \sin\theta}{a_1 + 1} \Pi\left[-\frac{2\sin\theta(a_1 + 1)}{a_{31}(1 - \sin\theta)}, k\right] \right\},$$

$$I_5(x') = \frac{\sqrt{a_{31}a_{42}}}{2(x^2 - 1)(x'^2 - 1)} [(2 - k^2)K(k) - 2E(k)],$$

$$I_6(x') = \pi(|\cos\theta| - 1),$$

$$I_7(x') = \frac{2a_{41}}{\sqrt{a_{31}a_{42}}} \left\{ -\frac{a_{31}}{a_1 - 1} K(k) + \Pi\left(-\frac{2\sin\theta}{a_{31}}, k\right) + \frac{1 - \sin\theta}{a_1 - 1} \Pi\left[\frac{2\sin\theta(a_1 - 1)}{a_{31}(1 + \sin\theta)}, k\right] \right\}, \tag{86}$$

where the argument (x') of a_i, a_{rs}, and k (given by Equation (82)) has been omitted.

7. Behavior of the Solution at Significant Locations

Regarding the axial and reflection symmetries, one naturally asks whether and how the solution simplifies on the axis and in the equatorial plane. On the axis, $\sin\theta = 0$ and $\cos^2\theta = 1$, so, in the potential (81), $a_3 = 0$, $a_4 = 0$, and $k = 0$, so all the elliptic integrals there reduce to $\pi/2$ and

$$a_{31}a_{42} = a_{41}a_{32} = a_1 a_2 = x'^2 + x^2 - 1.$$

Finally, considering that the disk has to lie above the horizon, i.e., at $x' > 1$, we have $H(x'^2 - 1) = 1$, so the first term of Equation (81) is the same for both $x' = x_{\text{in}}$ and $x' = x_{\text{out}}$ (and thus cancels out), and hence

$$\nu_1(x, \theta = 0) = -2\pi MS\left(\sqrt{x_{\text{out}}^2 + x^2 - 1} - \sqrt{x_{\text{in}}^2 + x^2 - 1}\right). \tag{87}$$

Also, the equatorial form of the potential (81) is somewhat simpler, namely, the first term and the one with the Π integral vanish, so one is left with

$$\nu_1(x, \theta = \pi/2) = -2MS\left[\frac{(a_1 - 1)(a_2 + 1)E(k) + (x'^2 - x^2)K(k)}{\sqrt{(a_1 - 1)(a_2 + 1)}} \right]_{x'=x_{\text{in}}}^{x'=x_{\text{out}}}. \tag{88}$$

At radial infinity $(r \to \infty)$, the disk potential falls off as

$$\nu_1(r \to \infty) \propto -\frac{\pi S}{r} \left[r_{\text{out}}^2 - r_{\text{in}}^2 - \frac{M^4}{16}\left(\frac{1}{r_{\text{in}}^2} - \frac{1}{r_{\text{out}}^2}\right) \right], \tag{89}$$

and at the horizon $(x = 1)$, it assumes the value

$$\nu_1(x = 1, \theta) = -2\pi MS\left(\sqrt{x_{\text{out}}^2 - \sin^2\theta} - \sqrt{x_{\text{in}}^2 - \sin^2\theta}\right). \tag{90}$$

The formula for the dragging perturbation $\omega_1(x, \theta)$ is trickier and does not reduce as much on the axis and in the equatorial plane (however, Figure 3 shows that it behaves reasonably). Very simple limits can still be obtained at radial infinity, where it falls off as

$$\omega_1(x \to \infty) \propto \frac{W}{4} \frac{x_{\text{out}} - x_{\text{in}}}{x^3} \quad \Longrightarrow \quad \omega_1(r \to \infty) \propto \frac{WM^2}{4r^3}\left[r_{\text{out}} - r_{\text{in}} + \frac{M^2}{4}\left(\frac{1}{r_{\text{out}}} - \frac{1}{r_{\text{in}}}\right)\right], \tag{91}$$

and on the horizon, where it is everywhere the same (independent of θ) and with its sign given by W,

$$\omega_1(x = 1) \equiv \omega_H = \frac{W}{8} \frac{(x_{\text{out}} - x_{\text{in}})(x_{\text{out}} + x_{\text{in}} + 2)}{(x_{\text{out}} + 1)^2(x_{\text{in}} + 1)^2}. \tag{92}$$

8. Parameters of the Disk Source

In order to calculate the physical characteristics of the disk, we realize that all of the densities and one-stream pressure (σ, P, σ_+, σ_-) are themselves *small*, namely, of linear perturbation order (see Equation (30)), and that the geodesic orbital velocities (18) are given by their unperturbed Schwarzschild values ($\pm\Omega_0$, which corresponds to $v_+ = -v_- = v_0 = 2\sqrt{Mr}/(2r - M)$) plus the terms $O(\omega)$, where ω is (of course) linearly small. Consequently, up to the linear order, the relations (26)–(28) between normal jumps of the metric gradients across the disk and their physical parameters reduce to

$$\nu_{1,z}(z=0^+) = 2\pi(S^\phi_\phi - S^t_t) = 2\pi(\sigma + P)\frac{1 + v^2}{1 - v^2} = 2\pi(\sigma_+ + \sigma_-)\frac{1 + v_0^2}{1 - v_0^2}, \tag{93}$$

$$\omega_{1,z}(z=0^+) = -\frac{8\pi S^t_\phi}{B^2\rho^2 e^{-4\nu_0}} = -8\pi(\sigma + P)\frac{\Omega}{1 - v^2} = -8\pi(\sigma_+ - \sigma_-)\frac{\Omega_0}{1 - v_0^2}, \tag{94}$$

$$\zeta_{1,z}(z=0^+) = 4\pi S^\phi_\phi = 4\pi\frac{\sigma v^2 + P}{1 - v^2} = 4\pi(\sigma_+ + \sigma_-)\frac{v_0^2}{1 - v_0^2}. \tag{95}$$

Differentiating the potentials (83) and (81) across the disk plane and noting that $\nu_{,\theta}(\theta = \pi/2^-) = -r\nu_{,z}(z = 0^+)$, we find

$$\frac{\partial V}{\partial \theta}\bigg|_{\theta=\frac{\pi}{2}^-} = -2\pi MSx\, H(x' - x) \implies \nu_{1,z}(z=0^+) = 2\pi S\left(1 + \frac{M^2}{4r^2}\right) = \frac{2\pi SM}{r}\frac{1 + v_0^2}{v_0^2}, \tag{96}$$

(the result only applies where the disk actually lies, i.e., at $x_{\rm in} \leqslant \frac{r}{M} + \frac{M}{4r} \leqslant x_{\rm out}$; elsewhere, it is zero, of course), hence, according to Equation (93),

$$\sigma_+ + \sigma_- = \frac{\nu_{1,z}(z=0^+)}{2\pi}\frac{1 - v_0^2}{1 + v_0^2} = \frac{S}{4r^2}(4r^2 - 8Mr + M^2). \tag{97}$$

It is more involved to find the equatorial limit of the normal gradient of ω_1 (Equation (84)). One finds that it is solely the term $Q_7 I_7$ that eventually contributes, because $Q_5 I_5$ is zero from the beginning; the first separate term of Equation (84), as well as $Q_0 I_0$, is independent of θ; $Q_6 I_6$ is independent of x' (and thus its "out" and "in" values subtract to zero); the $Q_2 I_2$ and $Q_3 I_3$ terms vanish in the $\theta \to (\pi/2)^-$ limit; and the contributions of the terms $Q_1 I_1$ and $Q_4 I_4$ exactly cancel out each other in this limit. From $(Q_7 I_7)_{,\theta}$ one specifically obtains, in the above limit, non-zero terms,

$$\frac{2Q_7(a_1 + 1)}{\sqrt{(a_1 - 1)^3(a_2 + 1)}}\left[-\Pi(n, k)\cos\theta + (1 - \sin\theta)\frac{\partial\Pi(n, k)}{\partial\theta}\right], \quad \text{where} \quad n = n(x, x', \theta) := \frac{2\sin\theta(a_1 - 1)}{(1 + \sin\theta)(a_1 - \sin\theta)},$$

and where the derivative of $\Pi(n, k)$ contributes solely through the term $\frac{\Pi(n,k)}{2(1 - n)}\frac{\partial n(x, x', \theta)}{\partial\theta}$. Using the asymptotics

$$\Pi(n, k) \propto \frac{\pi\sqrt{n}}{2\sqrt{n - k^2}\sqrt{1 - n}} + O(1) \quad \text{valid for} \qquad n \to 1^-$$

in both terms and taking the equatorial limit, one finally finds the simple result

$$\lim_{\theta\to\frac{\pi}{2}^-}\frac{\partial\omega_1}{\partial\theta}\left(=-r\lim_{z\to 0^+}\frac{\partial\omega_1}{\partial z}\right) = \frac{W}{2}\frac{x - 1}{(x + 1)^3} = 8WM^2 r^2\frac{(2r - M)^2}{(2r + M)^6}, \tag{98}$$

which, when compared against

$$\lim_{z\to 0^+}\frac{\partial\omega_1}{\partial z} = -8\pi(\sigma_+ - \sigma_-)\frac{\Omega_0}{1 - v_0^2} = -8\pi(\sigma_+ - \sigma_-)\frac{8r\sqrt{Mr}}{(2r + M)^3}\frac{(2r - M)^2}{4r^2 - 8Mr + M^2},$$

given by Equation (94), implies that

$$\sigma_+ - \sigma_- = \frac{WM^2}{8\pi\sqrt{Mr}}\frac{4r^2 - 8Mr + M^2}{(2r + M)^3}. \tag{99}$$

By adding Equations (97) and (99), we then have

$$\sigma_\pm = \frac{4r^2 - 8Mr + M^2}{8r^2}\left[S \pm \frac{W(Mr)^{3/2}}{2\pi(2r + M)^3}\right]. \tag{100}$$

To find the one-stream disk characteristics, one first combines Equations (93) and (95), which yields

$$v^2 = \frac{\sigma v_0^2 - P}{\sigma - P v_0^2} = \frac{4Mr\sigma - (2r - M)^2 P}{(2r - M)^2\sigma - 4MrP}. \tag{101}$$

Substituting this for v^2 in Equation (94) leads to

$$(\sigma v_0^2 - P)(\sigma - P v_0^2) = (\sigma_+ - \sigma_-)^2 v_0^2,$$

and from there, using $\sigma - P = \sigma_+ + \sigma_-$, we find

$$\sigma = +\frac{\sigma_+ + \sigma_-}{2} + \sqrt{\left(\frac{\sigma_+ + \sigma_-}{2}\right)^2 + \frac{4\,\sigma_+\sigma_- v_0^2}{(1 - v_0^2)^2}} = +\frac{\sigma_+ + \sigma_-}{2} + \sqrt{\left(\frac{\sigma_+ + \sigma_-}{2}\right)^2 + \frac{16Mr(2r - M)^2\,\sigma_+\sigma_-}{(4r^2 - 8Mr + M^2)^2}}, \qquad (102)$$

$$P = -\frac{\sigma_+ + \sigma_-}{2} + \sqrt{\left(\frac{\sigma_+ + \sigma_-}{2}\right)^2 + \frac{4\,\sigma_+\sigma_- v_0^2}{(1 - v_0^2)^2}} = -\frac{\sigma_+ + \sigma_-}{2} + \sqrt{\left(\frac{\sigma_+ + \sigma_-}{2}\right)^2 + \frac{16Mr(2r - M)^2\,\sigma_+\sigma_-}{(4r^2 - 8Mr + M^2)^2}}. \qquad (103)$$

Note that when substituting these σ and P back into Equation (101), the resulting v given by the square root of the latter is to be taken with the $+/-$ sign in the case where $\sigma_+ > \sigma_-$ / $\sigma_+ < \sigma_-$.

In order to demonstrate that the procedure really works and, in particular, to illustrate the role of the parameters S and W, let us consider a disk spanning between the radii $\rho_- = 5M$ and $\rho_+ = 7M$ and surrounding a black hole of mass M. Let us plot the results for several different values of S and/or W. Note that both S and W have the dimension of 1/length, practically $1/M$. Note also that in order to emphasize their effect, we ignore here the assumption that the perturbation should be very small. More precisely, the first-order perturbation of the gravitational potential is in fact *not* restricted by this assumption, because rotation/dragging only enters in the second order, so the change of ν can be understood as an *exact* superposition within the non-rotating, static class. The potential ν (the sum of the Schwarzschild background ν_0 and the perturbation ν_1) is shown in Figure 2; it behaves in an expected manner, namely, that the disk effect grows with increasing S (and is independent of W). The dragging angular velocity amounts to $\omega = \omega_1$ (since $\omega_0 = 0$), so the level-contour shape is in fact fixed and does not change with the parameters (only the level values do change; in particular, they scale with W); this is shown in Figure 3.

Now, we discuss the parameters of the double-stream and single-stream interpretations, i.e., $\sigma_\pm$ and $v_\pm$, and σ, P, and v, respectively. In fact, the orbital velocities $v_\pm$ of the double-stream picture need not be computed, since in the first perturbation order, they are the same as in a pure Schwarzschild field, because the field Equations (6) and (7) have their right-hand sides proportional to the surface densities, which are themselves of linear order. The other quantities are plotted in Figure 4 for several choices of the S and W parameters. One sees there that an increasing value of W makes σ_+ and σ_- more and more different, with σ_- finally becoming negative, which marks the limits of the (counter-)rotating interpretation. Physically, such a situation means that, for a given mass, the disk has too much angular momentum. Naturally, this is also accompanied by a need for a too-high orbital velocity; such a circumstance can be "remedied" by increasing the mass, i.e., S.

8.1. Mass and Angular Momentum of the Disk

The total mass and angular momentum of a stationary and axially symmetric spacetime can be found from Komar integrals, given by the Killing vector fields $\eta^\mu = \frac{\partial x^\mu}{\partial t}$ and $\xi^\mu = \frac{\partial x^\mu}{\partial \phi}$. In our case (involving two sources), the integrals over spatial infinity can be split into contributions from the black hole M and J (given by integration over the horizon H) and from the disk (integrated over some space-like hypersurface Σ covering the black hole exterior),

$$\text{mass} = \frac{1}{8\pi}\lim_{S\to\infty}\oint_S \eta^{\mu;\nu}dS_{\mu\nu} = \frac{1}{8\pi}\oint_H \eta^{\mu;\nu}dS_{\mu\nu} - \int_{\Sigma>H}(2T_\nu^\mu\eta^\nu - T\eta^\mu)d\Sigma_\mu = M + \int_{\Sigma>H}(T_i^i - T_t^t)\sqrt{-g}\,d^3x, \qquad (104)$$

$$\text{ang.m.} = -\frac{1}{16\pi}\lim_{S\to\infty}\oint_S \xi^{\mu;\nu}dS_{\mu\nu} = -\frac{1}{16\pi}\oint_H \xi^{\mu;\nu}dS_{\mu\nu} + \frac{1}{2}\int_{\Sigma>H}(2T_\nu^\mu\xi^\nu - T\xi^\mu)d\Sigma_\mu = J + \int_{\Sigma>H}T_\phi^t\sqrt{-g}\,d^3x, \qquad (105)$$

where we have finally employed the "Killing" coordinates t and ϕ in which $\eta^\mu = \delta_t^\mu$ and $\xi^\mu = \delta_\phi^\mu$, and a natural space-like section $\Sigma = \{t = \text{konst}\}$ (which corresponds to $d\Sigma_\mu = \delta_\mu^t\sqrt{-g}\,d^3x$). Clearly, $(T_i^i - T_t^t)$—or actually $e^{2\lambda-2\nu}(T_i^i - T_t^t)$—plays the same role as mass density in Newtonian theory. Note also that the second part of the mass integral represents what is sometimes called Tolman's formula.

Choosing $B = 1$, the metric determinant reads $-g = \rho^2 e^{4\lambda-4\nu}$, so, if the thin $\{z = 0\}$-disk is considered as the source and thus having $T_\nu^\mu\sqrt{-g} = S_\nu^\mu\rho\,\delta(z)$, the disk mass and angular momentum (denoted by $\mathcal{M}$ and $\mathcal{J}$) come out as

$$\mathcal{M} = 2\pi\int_{\text{disc}}(S_\phi^\phi - S_t^t)\rho\,d\rho, \qquad \mathcal{J} = 2\pi\int_{\text{disc}}S_\phi^t\rho\,d\rho.$$

Substituting here for Equation (4) with $u^\phi = u^t\Omega$ and $u_\phi = g_{\phi\phi}u^t(\Omega - \omega)$, we have

$$S_\phi^t = (\sigma + P)(u^t)^2 g_{\phi\phi}(\Omega - \omega), \; S_\phi^\phi - S_t^t = (\sigma + P)(u^t)^2[e^{2\nu} + g_{\phi\phi}(\Omega^2 - \omega^2)] = \sigma + P + 2\Omega S_\phi^t, \qquad (106)$$

hence

$$\mathcal{M} = 2\pi\int_{\text{disc}}(\sigma + P + 2\Omega S_\phi^t)\rho\,d\rho, \qquad (107)$$

$$\mathcal{J} = 2\pi\int_{\text{disc}}(\sigma + P)\frac{\rho e^{-2\nu}(\Omega - \omega)}{1 - \rho^2 e^{-4\nu}(\Omega - \omega)^2}g_{\phi\phi}\,d\rho; \qquad (108)$$
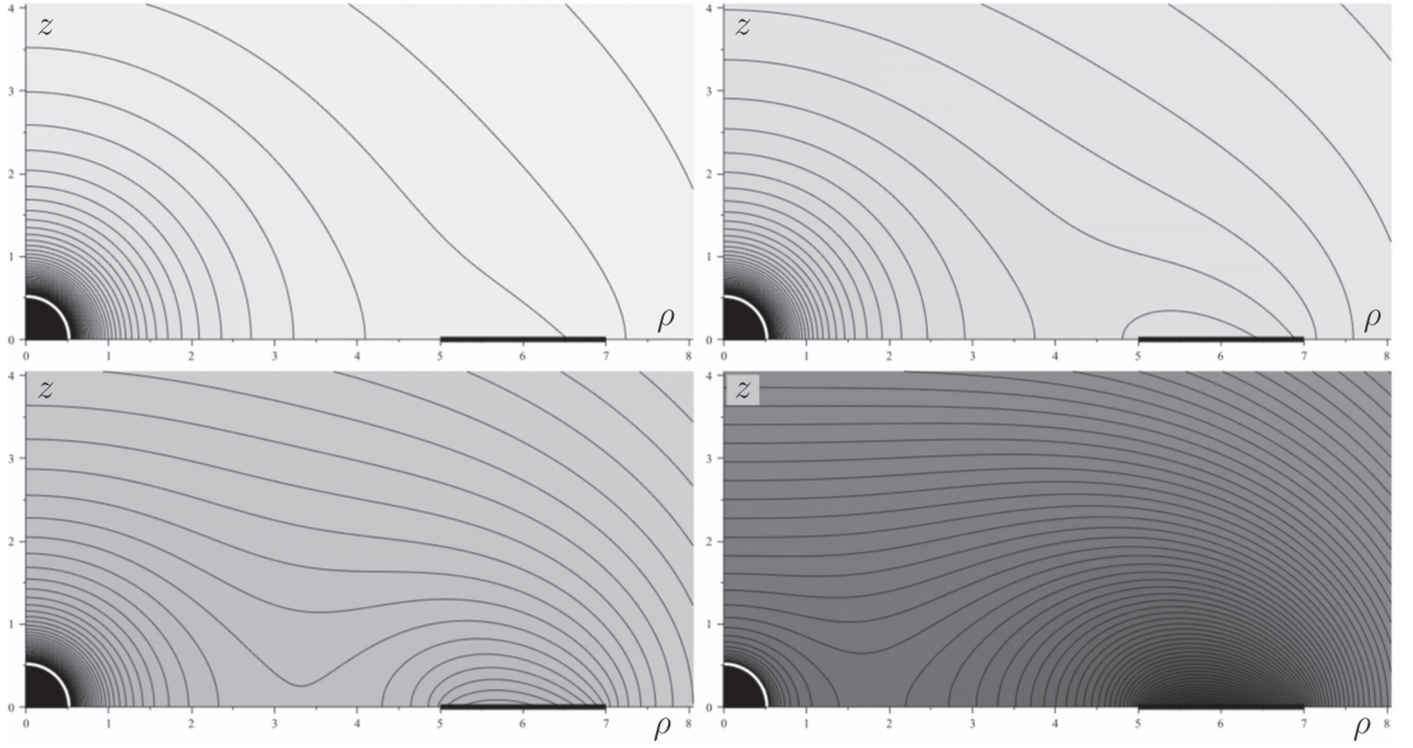
Figure 2. Meridional-plane contours of the gravitational potential ν, given by the sum of the Schwarzschild expression and the contribution from the disk. The four examples shown represent an equatorial disk stretching from $\rho = 5M$ to $\rho = 7M$ (it is indicated by a thick black line), with the potential (81) scaled by $S = 0.01$ (top left), $S = 0.026$ (top right), $S = 0.1$ (bottom left), and $S = 1.0$ (bottom right) (such a series corresponds to an increasingly massive disk). The potential is everywhere negative, with light/dark shading indicating shallow/deeper values (the potential diverges to $-\infty$ at the horizon, while the "weakest" levels reached at the top-right corners of the plots amount to -0.20 at the top left, to -0.34 at the top right, to -1.00 at the bottom left, and to -8.96 at the bottom right); the black hole horizon (at $\rho^2 + z^2 = M^2/4$) is represented by the white quarter-circle. Both axes are given in units of M.

in the special case of $\Omega = \mathrm{const}$, the first integral amounts to

$$\mathcal{M} = 2\pi \int_{\mathrm{disc}} (\sigma + P)\rho \, d\rho + 2\Omega \mathcal{J}.$$

One can alternatively express, in the integrals, S_ν^μ in terms of jumps of the normal fields, according to Equations (26)–(27). Setting $B = 1$ again, we thus have

$$S_\phi^t = -\frac{1}{8\pi} \rho^2 e^{-4\nu} \omega_{,z}, \qquad S_\phi^\phi - S_t^t = \frac{\nu_{,z}}{2\pi} + 2\omega S_\phi^t,$$

hence

$$\mathcal{M} = \int_{\mathrm{disc}} \left(\nu_{,z} - \frac{1}{2} \rho^2 e^{-4\nu} \omega \omega_{,z} \right) \rho \, d\rho, \quad \mathcal{J} = -\frac{1}{4} \int_{\mathrm{disc}} \rho^3 e^{-4\nu} \omega_{,z} \, d\rho \tag{109}$$

(where $\omega_{,z}$ and $\nu_{,z}$ are evaluated at $z \to 0^+$). Since the second term in $\mathcal{M}$ is $O(\lambda^2)$, in the linear order one is left with just

$$\mathcal{M}_1 = \int_{\mathrm{disc}} \nu_{1,z}(z \to 0^+)\rho \, d\rho, \quad \mathcal{J}_1 = -\frac{1}{4} \int_{\mathrm{disc}} \rho^3 e^{-4\nu_0} \, \omega_{1,z}(z \to 0^+) \, d\rho. \tag{110}$$

Finally, one has to realize that the above formulas hold for $B = 1$, whereas our results for ν_1 and ω_1 have been derived with $B = 1 - \frac{M^2}{4r^2}$. However, adapting the integrals to the latter choice practically means just writing $B\rho$ instead of ρ in both integrands, reaching

$$\mathcal{M}_1 = \int_{\mathrm{disc}} B\rho \, \nu_{1,z}(z \to 0^+) \, d\rho, \quad \mathcal{J}_1 = -\frac{1}{4} \int_{\mathrm{disc}} B^3 \rho^3 e^{-4\nu_0} \, \omega_{1,z}(z \to 0^+) \, d\rho. \tag{111}$$

Considering specifically the above constant-density disk, it is clear from Equations (81) and (84) that $\mathcal{M}_1$ is scaled by the free parameter S while $\mathcal{J}_1$ is scaled by the second parameter W. We have from Equations (96) and (98), at $z \to 0^+$ (i.e., $\theta \to \pi/2^-$),

$$\nu_{1,z}\rho = -\nu_{1,\theta} = \pi S \left(2r + \frac{M^2}{2r} \right), \quad \omega_{1,z}\rho = -\omega_{1,\theta} = -8WM^2 r^2 \frac{(2r - M)^2}{(2r + M)^6}, \tag{112}$$
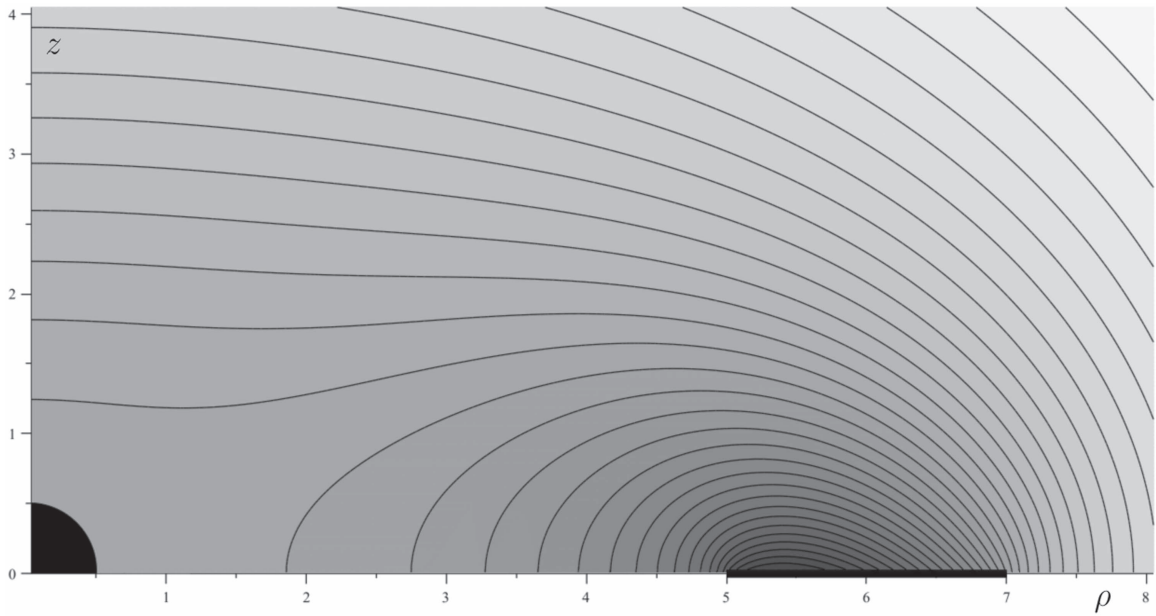
Figure 3. Meridional-plane contours of the dragging angular velocity ω, as entirely given by the first-order perturbation due to the disk (ω_1). The disk again stretches from $\rho = 5M$ to $\rho = 7M$ (as indicated by the thick black line). The angular velocity is everywhere positive, with light/dark shading indicating smaller/larger values (they reach about $0.0268/M$ at the disk and fall off to some $0.0047/M$ at the top right of the plot); the black quarter-disk at $\rho^2 + z^2 \leqslant M^2/4$ represents the black hole. Both axes are given in units of M. Since $\omega = \omega_1$ is proportional to W, the isolines have the same shape for any W; only their values scale with this rotational parameter.
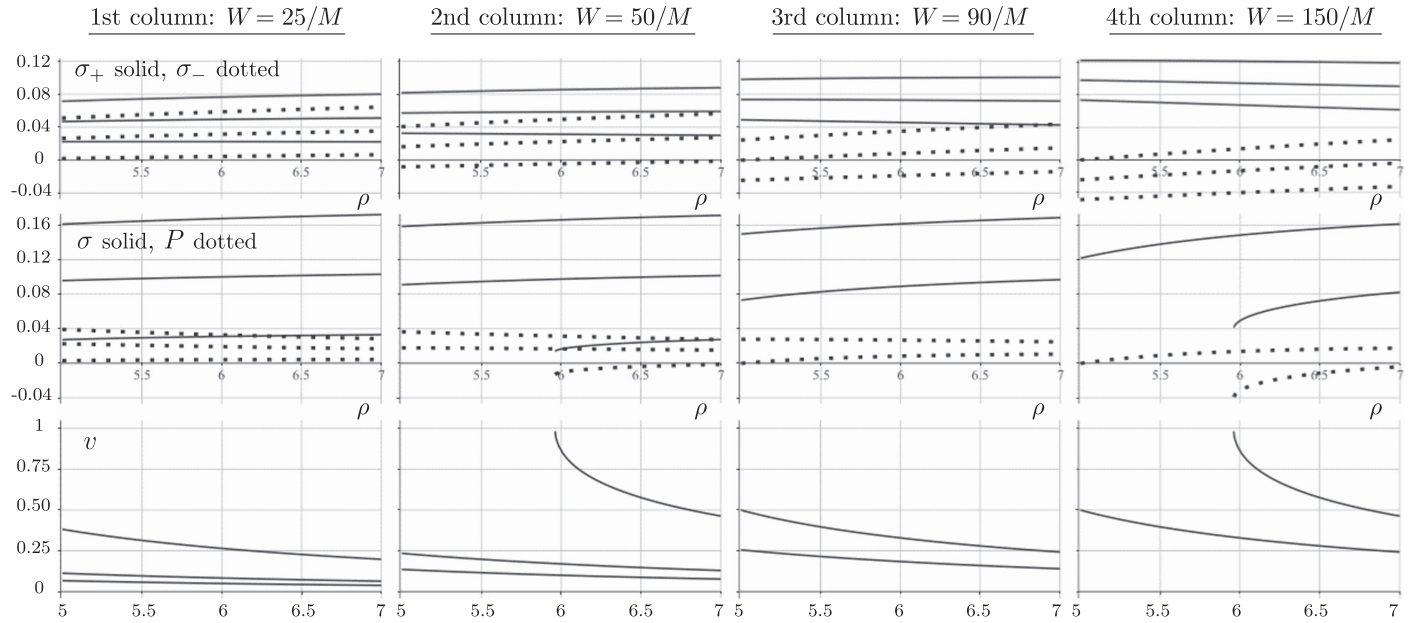

Figure 4. Parameters of the disk's double-stream and single-stream interpretations, plotted as functions of the Weyl radius for a disk stretching between $\rho = 5M$ and $\rho = 7M$ and for several combinations of the parameters S (Newtonian density) and W (scaling the disk rotation). The first/second/third/fourth columns represent the cases given by $W = 25/50/90/150$, with the first row showing the densities σ_+ (solid line), and σ_- (dotted line) of the double-stream, counter-rotating dust interpretation, the second row showing the density σ (solid line) and azimuthal pressure P (dotted line) of the single-stream fluid interpretation, and the third row showing the corresponding "bulk" velocity of the fluid v (solid). For each of the values of W, three different values of S were chosen, corresponding to disks of different masses—$S = 0.04$, 0.12, and 0.2. The density and pressure curves obtained for higher S are higher (given by larger values), whereas the corresponding bulk velocities decrease with growing S. The ranges of the chosen W and S are largely out of the scope of the linear perturbation, but this is in order to illustrate clearly what they represent. Since all of the parameters (densities, pressure, velocity) should be real and positive and the velocity v has to be <1 in addition, one sees immediately that (i) the disks with a given mass cannot bear any large angular momentum (with increasing W, the density σ_- of the double-stream interpretation—and consequently also the single-stream parameters—tend to be negative), and (ii) since a large W implies the need for high orbital velocities, for a too-large W, the orbital interpretation would have to involve superluminal motion (in the bottom row, from left to right, one sees that all three/two/two/one of the shown cases are "physical" in this respect). The densities S, W, σ_+, σ_-, and σ, as well as the pressure P, have the dimension of 1/length, and their values are in units of $1/M$; the speed v is dimensionless.

which yields, after using $\rho(\theta = \pi/2) = r$ and $e^{-4\nu_0} = \frac{(2r+M)^4}{(2r-M)^4}$,

$$\mathcal{M}_1 = \pi S \int_{r_{\text{in}}}^{r_{\text{out}}} \left(2r + \frac{M^2}{2r}\right)\left(1 - \frac{M^2}{4r^2}\right)dr = \pi S\left[r_{\text{out}}^2 - r_{\text{in}}^2 - \frac{M^4}{16}\left(\frac{1}{r_{\text{in}}^2} - \frac{1}{r_{\text{out}}^2}\right)\right], \tag{113}$$

$$\mathcal{J}_1 = \frac{WM^2}{8} \int_{r_{\text{in}}}^{r_{\text{out}}} \left(1 - \frac{M^2}{4r^2}\right)dr = \frac{WM^2}{8}\left[r_{\text{out}} - r_{\text{in}} - \frac{M^2}{4}\left(\frac{1}{r_{\text{in}}} - \frac{1}{r_{\text{out}}}\right)\right]. \tag{114}$$

The same results follow from the asymptotics (89) and (91), with regard to the general behavior (in an asymptotically flat spacetime):

$$\nu(r \to \infty) \propto -\frac{M + \mathcal{M}_1}{r}, \quad \omega(r \to \infty) \propto 2\,\frac{J_1 + \mathcal{J}_1}{r^3}.$$

The last statement implies that (i) the black hole mass remains M (which should be so in the linear perturbation order), and that (ii) all of the angular momentum of the system (inferred from the asymptotic behavior of ω) is being carried by the disk, hence the angular momentum of the hole remains zero, $J = 0$. Actually, we can verify this directly by computing the respective Komar integral over the horizon. It is known that the latter can be rewritten (see, e.g., Will 1974, Equation (21)) as

$$J = -\frac{k^4}{2^7} \int_0^\pi [B^3\omega_{,r}\, e^{-4\nu}]_{r=k/2}\, \sin^3\theta\, d\theta,$$

where in our first-order case one takes $\nu = \nu_0$, $\omega = \omega_1$, and $k = M$. Inspecting the radial gradient $\omega_{1,r}$ of Equation (84), one finds that all of the terms of this expression individually vanish at the horizon (irrespective of θ), so the above formula really yields $J = 0$. Hence, the perturbed black hole is rotating with respect to the asymptotic inertial frame with non-zero (positive) angular velocity (92), but has zero angular momentum, which means that it is just being "carried along" by the dragging primarily induced by the disk. We stress that this feature is *not* a necessary outcome of the perturbation procedure, namely, it is a consequence of our choice of the constants J_l (namely $J_l = 0$), which can be employed to fix the black hole spin in the solution (50) of the inhomogeneous perturbation Equation (44); see the discussion in Section 3.1.

9. Concluding Remarks

We showed that the procedure suggested by Will (1974), originally employed to determine the gravitational perturbation of a Schwarzschild black hole by a slowly rotating and light thin ring, can also be applied to the perturbation due to a thin disk. However, concerning the bad numerical properties of the series involved, we dropped the angular expansion and instead expressed the Green's functions (perturbations due to a thin ring) in closed form. Such expressions bring more complex special functions, but these can be evaluated effectively with rapidly converging algorithms, so the resulting numerical convergence is much better.

Using the proposed closed-form Green's functions, one can in principle obtain an arbitrary order of the perturbation. However, numerical treatment is necessary in order to analyze specific results, as illustrated on a simple example of the "uniform-density" disk in Section 6.

An important point has been to show that the series involved in the computation of the Green's functions converge (Section 4 and the accompanying paper by P. Čížek 2017, in preparation). However, what still remains to be answered is whether the perturbation scheme is effective to *any* order, namely, whether the perturbation expansion (29) with the parameter proportional to the external-source mass converges. Regarding the structure of the Green's functions and the speed of their convergence to zero at infinity, as well as the structure of source terms of higher perturbation orders, one conjectures that the expansion converges at least for some positive disk masses.

Various properties of the obtained solution could be studied now, for instance, the deformation of the geometry (as represented by curvature invariants, in particular), deformation of the (originally spherical) horizon, perturbation of the properties of stationary circular motion, or influence on the geodesic structure. In particular, it will be interesting to see how the perturbation influences the location of important circular equatorial geodesics (mainly of the innermost stable one, usually abbreviated as ISCO), because this should indicate how the actual quasi-stationary accretion disk may differ from its test-matter model. Also, a propos, one could consider a different type of disk (a different density distribution)—preferably close to what follows from models of accretion onto astrophysical black holes—and compare the results with what has been found here for the simplest case of constant density.

9.1. Comparison with Black Hole–Disk Configurations Found Numerically

Another obvious option is to compare the perturbative solution with the results of the numerical treatment of similar source configurations. The most similar of these—a hole with a thin finite annular equatorial disk—was studied by Lanza (1992), while Nishida & Eriguchi (1994) considered a hole with a thick toroid. More recently, Ansorg & Petroff (2005) used a different numerical method to compute stationary and axisymmetric configurations of uniformly rotating constant-density toroids around black holes. They specifically used these solutions to demonstrate that both the central hole and the surrounding toroid may in some cases have *negative* Komar masses (Ansorg & Petroff 2006). Other codes for studying self-gravitating matter around black holes have been developed and specifically used to find stationary thick-toroid configurations by Shibata (2007), Montero et al. (2008), and

Stergioulas ([2011](#)). Finally, Karkowski et al. ([2016](#)) analyzed such rotating black hole–toroid systems in the first post-Newtonian approximation.

The possibility of comparing our results with the above "exact" numerical configurations (in particular the thin disks by Lanza) is very limited, mainly because our first-order perturbation only represents the gravitation of the disk, not its *self*-gravitation (no back effect of the source on itself through its field); more generally speaking, the solution does not incorporate any nonlinearity of the Einstein equations. There are also other, more definite differences. The numerical results of Lanza ([1992](#)) were obtained by numerical "relaxation" of the initial configurations provided by "squeezing" the well-known (analytical) *test* thick-disk models in a given Kerr background. More specifically, assuming a constant ratio of angular momentum to energy (with respect to infinity) throughout the disk, in our notation

$$\text{const} = \frac{u_\phi}{-u_t} = -\frac{g_{t\phi} + g_{\phi\phi}\Omega}{g_{tt} + g_{t\phi}\Omega} = \left(\omega + \frac{e^{2\nu}}{B\rho\, v}\right)^{-1},$$

and choosing the inner disk radius and the proportionality constant appearing in the polytropic equation of the disk-gas state, the initial surface density and outer radius of the disk are obtained. Generally, with the increase of that constant, the surface density (as well as pressure) and mass of the resulting disk rise quickly, while the outer disk radius grows with the specific angular momentum of the disk matter. In contrast to Lanza's constraint of constant specific angular momentum, and the disk's surface density and outer radius derived accordingly, we showed our perturbation procedure on a disk with a prescribed and constant Newtonian surface density (while having a non-constant angular momentum) and with both inner and outer radii prescribed as well.

Lanza illustrated his numerical scheme on two groups of configurations sequences, one containing a rapidly rotating hole (specified by its horizon area and angular momentum) and one with a slowly rotating hole (in this case specified by its horizon angular velocity ω_H and isotropic radius $k/2$). Focusing naturally only on the latter, one finds solution sequences for three different rotation choices in the cited paper: $\omega_H = 0.00025/M$, $\omega_H = 0.0025/M$, and $\omega_H = 0.025/M$, in all cases with $k = M$ and $r_{\rm in} = 8M$; each sequence is characterized by a certain fixed value of the angular momentum to energy ratio (constant throughout the disk) and was generated by the gradual increase of the disk mass. With increasing disk mass, the total mass of the system was also found to increase (almost linearly), while the total angular momentum and the horizon area A_H were increasing slightly faster, with the horizon surface gravity consequently decreasing according to the generic relation $\kappa_H = 4\pi k/A_H$. One special point Lanza examined on slowly rotating configurations was that the black hole rotational angular momentum may decrease to negative values when the disk angular momentum is being increased (while ω_H is kept fixed). This happens when the disk is "overtaking" the black hole in the sense that the combined rotational-dragging effect is stronger than the effect due to the hole alone (such a circumstance was already pointed out by Will [1974](#)). Let us remind the reader that in our case the black hole was effectively *set* to keep zero angular momentum (while acquiring non-zero angular velocity) in the perturbation, as confirmed at the end of Section [8.1](#).

Regarding the differences between the assumptions of the above numerical treatment and our perturbative one, a comparison of the results obtained by these two methods is going to be rather problematic. Anyway, we now plan to compute the various, more specific parameters of the disk considered as an example in Section [6](#) (and in the following sections) in order to possibly return to this point. Let us thus conclude with one particular surprising observation made by Lanza ([1992](#)), which should be simple to compare against: for slowly rotating black holes, Lanza found that the presence of the disk can make the horizon's polar proper circumference *larger* than the equatorial one, which would suggest that the horizon becomes prolate (along the symmetry axis). This goes against common experience that the black holes stretch toward external sources of gravity (cf. Nishida & Eriguchi [1994](#) and Ansorg & Petroff [2005](#) who always obtained oblate horizons).

ORCID iDs

O. Semerák ⬤ https://orcid.org/0000-0002-1272-6779

References

Abramowicz, M. A., Curir, A., Schwarzenberg-Czerny, A., & Wilson, R. E. 1984, MNRAS, 208, 279
Ansorg, M., & Petroff, D. 2005, PhRvD, 72, 024019
Ansorg, M., & Petroff, D. 2006, CQGra, 23, L81
Baranov, A. S. 2006, Math. Notes, 80, 167
Bardeen, J. M. 1973, in Rapidly Rotating Stars, Disks, and Black Holes, ed. C. DeWitt & B. S. DeWitt (New York: Gordon and Breach), 241
Bičák, J., & Ledvinka, T. 1993, PhRvL, 71, 1669
Bičák, J., Lynden-Bell, D., & Katz, J. 1993, PhRvD, 47, 4334
Bretón, N., Denisova, T. E., & Manko, V. S. 1997, PhLA, 230, 7
Bretón, N., García, A. A., & Manko, V. S. 1998, PhRvD, 57, 3382
Chaudhuri, S., & Das, K. C. 1997, JMP, 38, 5792
Chrzanowski, P. L. 1976, PhRvD, 13, 806

Čížek, P. 2011, J. Phys. Conf. Ser, 314, 012071
Čížek, P., & Semerák, O. 2009, in Proc. 18th Annual Conf. of Doctoral Students, Thin-disc Perturbation of a Schwarzschild Black Hole, WDS 2009, ed. J. Šafránková & J. Pavlů (Prague: Matfyzpress), 38
Demianski, M. 1976, GReGr, 7, 551
García-Reyes, G., & González, G. A. 2004, CQGra, 21, 4845
González, G. A., & Espitia, O. A. 2003, PhRvD, 68, 104028
Grandclément, P., & Novak, J. 2008, LRR, 12, 1
Hod, S. 2014, EPJC, 74, 2840
Hod, S. 2015, EPJC, 75, 541
Karkowski, J., Mach, P., Malec, E., Piróg, M., & Xie, N. 2016, PhRvD, 94, 124041
Kato, S., Fukue, J., & Mineshige, S. 2008, Black-Hole Accretion Disks. Towards a New Paradigm (Kyoto: Kyoto Univ. Press)
Klein, C., & Richter, O. 1999, PhRvL, 83, 2884
Klein, C., & Richter, O. 2005, Ernst Equation and Riemann Surfaces: Analytical and Numerical Methods (Berlin: Springer), 685
Krori, K. D., & Bhattacharjee, R. 1990, JMP, 31, 147
Lamberti, P. W., & Hamity, V. H. 1989, GReGr, 21, 869
Lanza, A. 1992, ApJ, 389, 141

Lass, H., & Blitzer, L. 1983, CeMec, 30, 225

Lynden-Bell, D., & Pineault, S. 1978, MNRAS, 185, 679

Meinel, R., Ansorg, M., Kleinwächter, A., Neugebauer, G., & Petroff, D. 2008, Relativistic Figures of Equilibrium (Cambridge: Cambridge Univ. Press)

Montero, P. J., Font, J. A., & Shibata, M. 2008, PhRvD, 78, 064037

Morgan, T., & Morgan, L. 1969, PhRv, 183, 1097

Nishida, S., & Eriguchi, Y. 1994, ApJ, 427, 429

Olver, F. W. J., Lozier, D. W., Boisvert, R. F., & Clark, C. W. (ed.) 2010, NIST Handbook of Mathematical Functions (Cambridge: Cambridge Univ. Press)

Ruggiero, M. L. 2016, Ap&SS, 361, 140

Sano, Y., & Tagoshi, H. 2014, PhRvD, 90, 044043

Semerák, O. 2002, CQGra, 19, 3829

Semerák, O. 2003, CQGra, 20, 1613

Semerák, O. 2004, CQGra, 21, 2203

Semerák, O. 2016, PhRvD, 94, 104021

Shibata, M. 2007, PhRvD, 76, 064035

Stergioulas, N. 2011, IJMPD, 20, 1251

Suková, P., & Semerák, O. 2013, MNRAS, 436, 978

Tomimatsu, A. 1984, PhLA, 103, 374

Will, C. M. 1974, ApJ, 191, 521

Will, C. M. 1975, ApJ, 196, 41

Zellerin, T., & Semerák, O. 2000, CQGra, 17, 5103